Cement 18 (2024) 100118

Contents lists available at ScienceDirect

Cement

journal homepage: www.sciencedirect.com/journal/cement

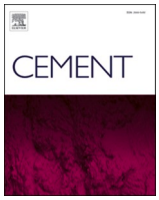

Accelerating effect of low replacements of carbonaceous materials in cement paste and mortar

Victor Brial, Thomas Duplessis, Claudiane M. Ouellet-Plamondon *

Department of Construction Engineering, École de Technologie Supérieure, Université du Québec, Canada

ARTICLE INFO

Keywords:
Cement hydration
Graphite
Activated charcoal
Carbon black
Mortar

ABSTRACT

This study investigated the effect of incorporating small amounts of carbonaceous materials in cement paste and mortar systems at a low dosage. The materials studied include industrial graphite, natural graphite, carbon black, activated charcoal, and decolorized charcoal. The effect of this material on cement hydration through different techniques such as compressive strength mortar, TGA, SEM, isothermal calorimetry, rheology, and calcium isotherm adsoprtion. These tests studied the influence of carbonaceous materials' properties on cement hydration. With the exception of industrial graphite G1, the carbonaceous materials showed an acceleration of setting after 1 day by favoring the nucleation of hydrates, reducing the porosity, and improving the mechanical properties. On the other hand, traces of this acceleration are no longer visible beyond 28 days. The accelerating effect of different carbons sources appears to be less dependent of crystallinity, mineralogy, or particle size, but rather on surface chemistry and the quality of particle dispersion.

1. Introduction

The concrete industry is one of the highest emitters of greenhouse gases as over 2.9 Gt of CO_2 were emitted by the cement industry in 2021 [1]. These emissions can hardly be decreased as they mainly result from the decarbonation of calcite during cement production [2]. Therefore, it remains complex to provide alternatives to reduce the carbon footprint of concrete and meet the objectives of the Paris agreement. The increased interest for high efficiency concrete and for viable alternatives to reduce the carbon footprint of concrete [3,4] has implemented a new dimension to the study of materials believed to improve concrete performance.

The primary motivations for this study were to understand the effects of low contamination of cementitious materials by carbonaceous materials, such as graphite, which can be present as impurities in new supplementary cementitious materials (SCMs) [5–8]. Moreover, the functionality of concrete, including properties like electrical conductivity, can be enhanced by incorporating carbonaceous materials [9,10]. While these materials have been well studied at higher dosages, their effects at low dosages remain less understood, especially in terms of hydration and early-age performance. Understanding the impact of low levels of carbonaceous materials can help in optimizing their use in practical applications where only small amounts are feasible or where unintentional contamination occurs.

Particularly the use of carbon-based nanomaterials such as graphene [11], graphene oxide [12], or carbon quantum dots have been investigated with the intention to reduce the cement content [13]. The use of these materials in concrete provided improvements on their durability or microstructure [13,14]. However, the use of nanomaterials at an industrial scale is complex as reaching the adequate unfavorable dispersion of nanomaterials in cementitious materials is necessary and essential [11,12]. Other unconventional materials like stainless steel powder or graphite were also studied, which enabled the discovery of concretes with new properties, such as conductive concretes [15]. Despite the effect on cementitious materials displayed by the use of carbon-based materials in concrete, carbonaceous materials' effects on cement hydration were partially studied compared to nanomaterials. Currently, it is known that the addition of 10 % to 20 % of graphite showed decreased mechanical performance through a reduction in heat released by calorimetry [9]. The analysis conducted by Dutta, Bordoloi, and Borthakur [16], included studies on setting time, compressive strength, hydration using XRD, and microstructure using SEM, thereby advancing knowledge on the impact of coal or coke on cement hydration. That study showed a decrease in mechanical performance after the addition of 15 % of coke or coke charcoal. Such decreased performance was mainly due to an increase in the porosity of the cement paste [16].

* Corresponding author at: École de technologie supérieure, 1100, rue Notre-Dame Ouest, Montréal (Québec) Canada H3C 1K3.
E-mail address: claudiane.ouellet-plamondon@etsmtl.ca (C.M. Ouellet-Plamondon).

https://doi.org/10.1016/j.cement.2024.100118
Received 30 May 2024; Received in revised form 30 August 2024; Accepted 24 September 2024
Available online 30 September 2024
2666-5492/© 2024 The Authors. Published by Elsevier B.V. This is an open access article under the CC BY-NC license (http://creativecommons.org/licenses/by-nc/4.0/).

Other experiments focused on different carbonaceous materials like activated carbon [17]. The results showed that the use of a small proportion of activated carbon improved mortar performance by reducing the porosity of the mix. On the other hand, beyond the 2 % addition of activated carbon, the mechanical properties decreased [17]. The studies analyzing the addition of carbonaceous materials in cement have mainly shown effects on porosity. However, the origin of these microstructure modifications is not currently well understood.

The present study aims to understand the impact of adding different types of carbonaceous materials on cement hydration and/or characterize potential improved performances of cement in the presence of the carbonaceous materials. This article aims to answer the following questions:

(i.) How does the addition of carbonaceous materials at low dosage in cement affect cement hydration?
(ii.) How does carbonaceous material properties affect the hydration of cement?

To answer this question, five carbon materials were tested: industrial graphite, natural graphite, activated carbon, carbon black, and decolorized carbon. These materials have been tested at replacement levels of 0.1 %, 0.5 %, 1 % and 2 %. The samples created with different replacement levels were tested with six different methods to answer both questions seen above. First, the influence of carbonaceous materials on the rheological properties of cement pastes was studied. The influence of the addition of carbon on the mechanical properties was then evaluated through compression tests on mortar. The influence of carbons on the amount of air in hardened mortar was also studied by image analysis. The impact of carbons on cement chemistry was assessed through isothermal calorimetry tests. In addition, thermogravimetry was performed to study cement chemistry on mixes containing 2 % carbon. Finally, the porosity was also evaluated on pastes containing 2 % carbon using scanning electron microscopy images in order to understand the impact of carbons on the microstructure of cement pastes.

2. Materials and methods

2.1. Materials

In this study, Portland cement (Type GU) was used to prepare the cement paste and mortar samples. Five carbonaceous materials were studied in this article. G1 is an industrial type graphite similar to graphite used to produce electrodes. This type of graphite is obtained by cooking pure coke at high temperature, G2 is a natural graphite flake with 99.9 % purity (metal basis). AC is a commercial grade activated charcoal with some impurities. CB is a carbon black Vulcan XC500 from Cabot. Finally, DC is a laboratory grade decolorized charcoal composed of pure activated charcoal. The chemical composition of the Portland cement was analyzed by X-ray fluorescence (XRF) bed fusion after loss of ignition of 30 min at 1000 °C. The chemical composition of Portland cement is shown in Table 1.

The mineralogical composition of Portland cement and the carbonaceous materials used in this paper were analyzed through X-ray powder diffraction (XRD) by Rietveld analysis. In addition to the previous measures, a zincite (ZnO) external standard was analyzed under the same method to determine the amorphous content. The diffractograms acquired for each of the carbonaceous materials are presented in Fig. A1 of the Appendix. The quantitative mineralogical compositions of the cement and the carbonaceous material powders studied are presented in Table 2.

Most of the carbonaceous materials tested are mainly composed of amorphous phases. For graphite, industrial graphite G1 is predominantly composed of amorphous carbons, as opposed to natural graphite G2, showing respective amorphous proportions of 81 % and 10 %. Regarding other carbon derivatives, black carbon CB, and decolorized carbon DC are composed entirely of amorphous carbon. Interestingly, in addition to its dominant amorphous carbon content, commercial activated carbon AC also shows 7.5 % quartz and 2.4 % calcite. This type of contamination is expected in commercial activated charcoal as shown by Ramirez-Gutierrez et al. [18].

The particle size of the carbonaceous materials tested was measured using a Malvern Mastersizer 3000 laser particle sizer with isopropanol as the dispersant. To ensure optimal dispersion, about 500 mg of carbonaceous materials were dispersed for 15 min in 50 mL of isopropanol using an ultrasonic bath. Drops of the previously dispersed solution obtained were then added to the isopropanol of the laser granulometer in order to obtain a filling between 5 % and 10 %. The volume density of the particles of Portland cement and of the various carbonaceous materials is presented in Fig. 1. Industrial graphite G1 and commercial activated carbon AC show a grain size similar to cement with d_{50} around 17 μm. Natural graphite G2, due to the flake shape of its grains, shows a slightly larger particle size seen by a d_{50} around 50 μm. On the other hand, the decolorized carbon DC and the carbon black CB show much finer grain sizes with a d_{50} of 1 μm and 0.17 μm respectively. In addition, grain-shaped observations of carbonaceous materials were made by scanning electron microscopy in secondary electron mode. These observations are visible in Fig. A2 in the Appendix. The specific surface area (SSA) values, as determined by BET analysis are presented Table 2. The Portland cement exhibits a relatively low SSA of 1.3 m^2/g, which is consistent with its larger particle size compared to the carbonaceous additives. Industrial graphite G1, with a d50 of approximately 17 μm, has a moderate SSA of 8.6 m^2/g, reflecting its relatively larger and more crystalline structure. Natural graphite G2, despite its larger d50 of 50 μm, shows a lower SSA of 4.8 m^2/g, which aligns with its flake-like morphology that offers less surface area per unit mass. In contrast, the highly porous nature of activated carbon AC, with a d50 of 17 μm, results in an exceptionally high SSA of 1265.6 m^2/g, indicating extensive internal porosity. Carbon black CB, with a much finer d50 of 0.17 μm, has a significant SSA of 237.3 m^2/g, highlighting the influence of its small particle size and high surface activity. Decolorized carbon DC, with a d50 of 1 μm, also demonstrates a high SSA of 823.1 m^2/g,

Table 2
Major mineralogical compositions,and BET surface area of the OPC, LCLL Ash and quartz powder.

Phase (wt%)	OPC	G1	G2	AC	CB	DC
C_3S	63.4	–	–	–	–	–
C_2S	7.3	–	–	–	–	–
C_3A	3.9	–	–	–	–	–
C_4AF	13	–	–	–	–	–
Quartz	–	–	–	7.5	–	–
Calcite	2.2	–	–	2.4	–	–
Graphite	–	19.1	89.7	3.4	–	–
Amorphous	–	80.9	10.3	86.7	100	100
SSA_{BET}	1.3	8.6	4.8	1265.6	237.3	823.1

Table 1
Chemical compositions of the cement.

	Percentage in weight (wt%)											
Oxide	SiO_2	Al_2O_3	Fe_2O_3	CaO	MgO	SO_3	K_2O	Na_2O	TiO_2	P_2O_5	V_2O_5	LOI
OPC	19.17	4.69	3.61	61.52	2.4	3.98	1.06	0.25	0.25	0.14	0.01	2.62

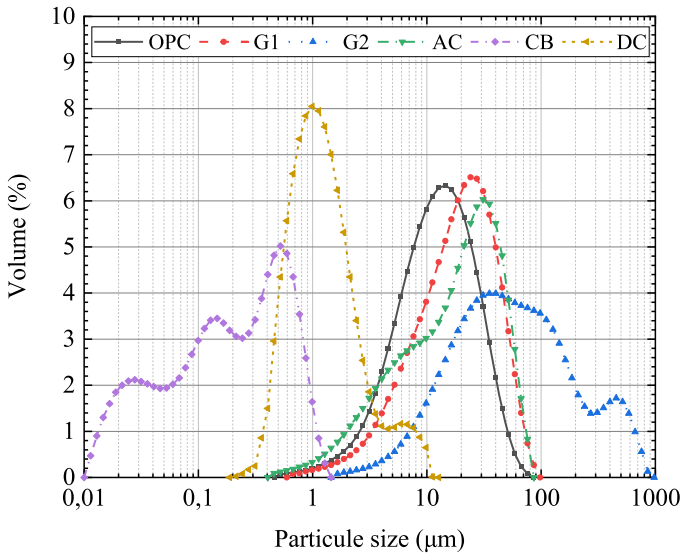

Fig. 1. Particle size analysis by laser granulometry of cement and carbonaceous materials tested.

reflecting its fine particle size and porous structure. These SSA values are coherent with the observed d50, where smaller particle sizes and higher porosity contribute to a greater specific surface area, thereby influencing the material's reactivity and interaction with the cement matrix.

2.2. Methods

2.2.1. Rheology

The effects on rheological properties were studied on cement pastes composed of 80 g of the mixture made of cement/carbonaceous material tested and 38.8 g of distilled water. Mixes with the following replacement levels of carbonaceous materials were made: 0.1 %, 0.5 %, 1 % and 2 %. The cement pastes were mixed according to the ASTM C1738 standard [19]. The rheological properties were measured using the same method as [5] with the 3D printed geometry recommended by NIST and previously calibrated with the SRM 2493 [20,21]. The measurements were taken 15 min after the initial contact between the distilled water and the cement on an Anton Paar MCR 302 rheometer. The data was recorded on a rising curve from 0.1 rpm to 100 rpm and a falling curve from 100 rpm to 0.1 rpm. Only the data from the 23 points of the downward curve were used. The shear stress τ, the shear rate $\dot{\gamma}$ and the apparent viscosity μ were calculated using Eqs. (1) to (3), by considering the rotational speed N and torque Γ measurements acquired. In these equations, the parameters Kτ and Kμ are determined when calibrating the geometry with the NIST reference material. In accordance with the NIST publication [21] the yield stress τ_0 and the plastic viscosity μ were calculated using the Bingham rheological model. Respectively, these were calculated as the ordinate at the origin and the slope from the linear regression of the curve $\tau=f(\dot{\gamma})$ where $(\dot{\gamma}) > 1\ s^{-1}$.

$$\tau = K\tau \times \Gamma \tag{1}$$

$$\dot{\gamma} = \frac{K\tau}{K\mu} \times N \tag{2}$$

$$\mu = K\mu \times \frac{\Gamma}{N} \tag{3}$$

Rheology was included in the study to evaluate the fresh state properties of the cement paste. Understanding how carbonaceous materials affect the rheological behavior provides insights into their influence on the dispersion of particles and, subsequently, on the hydration process. Proper dispersion can lead to improved nucleation of hydrates, which is an essential aspect of early-stage cement hydration [22].

2.2.2. Mortar compressive strength

The mortar samples were made and tested according to the ASTM C109 standard [23]. The mixes with the following replacement levels of carbonaceous materials were made: levels of 0.1 %, 0.5 %, 1 % and 2 %. In order to ensure homogeneity, the dispersion of carbonaceous materials was performed using a QSonica Q700 sonicator, with the materials being sonicated in a beaker filled with 100 mL of distilled water. The sonication duration was set to 15 min to ensure effective dispersion of the particles while avoiding excessive heating of the solution. Overheating could make the solution difficult to handle without heat protection gloves and could potentially affect the water temperature used in the mortar, thereby altering the hydration process during mixing [ref] . The mortar cubes were prepared according to the ASTM C305 standard [24] by mixing 3575 g of Ottawa sand, 1300 g of cement/carbonaceous material mix, and 650 ml of water. To maintain a constant water/binder ratio of 0.485 and a constant flow of 110 ± 5 [23], about 2 to 20 mL of polycarboxylate superplasticizer were used to limit the effect of different carbon particle sizes. The mortar mix proportions are presented in Table 3. Each mix was tested at 1, 7, 28, and 112 days. to evaluate the compressive strength activity index over time.

2.2.3. Hardened mortar air void measurement

Air void measurements in the hardened mortars were carried out after 28 days to assess the impact of the addition of a small proportion of carbonaceous material on the amount of air in the mortars. The air void measurements in the hardened state were carried out by image analysis according to the method proposed by Fonseca and Scherer [25] in accordance with ASTM C457 [26]. To proceed, three cubes of mortar were cut using a diamond saw through the middle in the direction perpendicular to the compaction. Each sample was then polished with 120, 320, 600, and 1000 grit SiC powders by water washing and air drying between each step. The polished surfaces thus obtained were then blackened using an indelible marker with a very broad tip and the air voids were contrasted by filling them with a white barium sulphate powder. The contrasting surfaces were then scanned using a commercial scanner with a resolution of 4800 ppi on a surface of 45×45 mm^2 in 16-bit grayscale. The images obtained were then analyzed with the MATLab procedure proposed by Fonseca et Scherer [25].

2.2.4. Isothermal calorimetry

Isothermal calorimetry tests were carried out according to the ASTM C1679 standard [27] on cement pastes with a water/binder ratio of 0.485. The water/binder ratio was selected to be consistent with the mortar mixes made according to the ASTM C109. These tests were performed with a TA Instrument TAMAir 8 channels isothermal calorimeter set at 23 °C with initial and final baselines recorded over 30 min. First 40 g of the cement/carbonaceous material mix was mixed with 19.4 g of distilled water for 2 min at 1600 rpm in a plastic tube. About 6.75 g of the resulting paste was then inserted into the ampoule of the calorimeter before being sealed. The reference ampoules were made with 16 g of Ottawa sand in order to maintain a heat capacity similar to the samples tested.

2.2.5. Thermogravimetric analysis (TGA)

The objective of the thermogravimetry tests was to evaluate the impact of the addition of carbonaceous materials on the chemical composition of the paste by analyzing the quantity of bound water in the hydrates. Only mixes with 2 % carbonaceous material replacement were submitted to this method to work with the samples providing the best visualization of carbon impact on cement's chemistry and to reduce the number of samples. The cement paste samples were prepared with the remaining paste from the calorimetry assay and molded in a plastic tube. Paste samples were demolded after 1 day and were then preserved in

Table 3
Mortar mix proportions and flow.

Mix	Materials					Flow (%)
	Cement	Carbonaceous materials	Sand	Water	superplasticizer	
Reference	1300		3575	630.5	–	108
Graphite G1						
0.1 % G1	1298.7	1.3	3575.0	630.5	2.0	111
0.5 % G1	1293.5	5.3	3575.0	630.5	2.7	107
1 % G1	1287.0	10.6	3575.0	630.5	6.2	115
2 % G1	1274.0	21.2	3575.0	630.5	3.9	110
Graphite G2						
0.1 % G2	1298.7	1.3	3575.0	630.5	5.5	113
0.5 % G2	1293.5	5.3	3575.0	630.5	7.0	114
1 % G2	1287.0	10.6	3575.0	630.5	6.6	107
2 % G2	1274.0	21.2	3575.0	630.5	7.8	105
Activated charcoal						
0.1 % AC	1298.7	1.3	3575.0	630.5	9.0	107
0.5 % AC	1293.5	5.3	3575.0	630.5	5.5	106
1 % AC	1287.0	10.6	3575.0	630.5	10.1	106
2 % AC	1274.0	21.2	3575.0	630.5	7.4	113
Carbon black						
0.1 % CB	1298.7	1.3	3575.0	630.5	10.1	106
0.5 % CB	1293.5	5.3	3575.0	630.5	8.2	110
1 % CB	1287.0	10.6	3575.0	630.5	11.7	113
2 % CB	1274.0	21.2	3575.0	630.5	21.5	106
Decolorized carbon						
0.1 % DC	1298.7	1.3	3575.0	630.5	5.9	115
0.5 % DC	1293.5	5.3	3575.0	630.5	12.9	107
1 % DC	1287.0	10.6	3575.0	630.5	16.8	108
2 % DC	1274.0	21.2	3575.0	630.5	17.6	106

lime water. After 1, 28 and 112 days in lime water, 3 g of each sample paste was submitted to hydration stoppage by solvent exchange with isopropanol and diethylether according to the method proposed by Snellings et al. [28] and Scrivener et al. [29]. Thermogravimetric analysis was carried out with a STA8000 from Perkins Elmer. For each test, approximately 50 mg of anhydrous sample was introduced into an alumina crucible. The mass loss was measured from 30 to 1000 °C with a heating rate of 10 °C/min with a dinitrogen flow of 50 mL/min. TGA tests were carried out in triplicates for each carbonaceous material mix tested and the reference. The DTG curves were calculated from the derivative of the curve of the evolution of mass as a function of temperature.

2.2.6. BSE electronic microscopy

The influence of carbonaceous materials on the microstructure of cement paste was studied by scanning electron microscopy (SEM) in backscattered electrons (BSE). Again, the reference and the mixes with 2 % carbonaceous material replacement were analyzed to limit the number of samples. As for the TGA tests, the cement paste samples were prepared with the rest of the paste from the calorimetry. Cylindrical specimens of cement paste hardened in lime water were sawed under cutting oil using a precision saw with a diamond blade to cut slides about 1.5 mm thick. The slides were rinsed in isopropanol and immersed in 100 ml of isopropanol for 48 h according to the procedure recommended by Scrivener, Snellings and Lothenbach [29]. After this procedure, the samples were vacuum dried and vacuum impregnated with a low viscosity epoxy resin to stabilize the microstructure. To ensure good quality BSE images, specimens were first lapped using 600 grit SiC paper and polished with 9 μm, 3 μm, 1 μm diamond paste using lapping oil as a lubricant. To avoid contamination from the previous polishing step, the sample was cleaned 15 min in isopropyl alcohol using an ultrasonic cleaner after each step. Before observing them under SEM, the samples were coated with 15 nm of carbon. Images were obtained with a Hitachi TM3030 tabletop SEM microscope equipped with a backscattered electron detector under an accelerating voltage of 15 kV with a x400 magnification. The samples were analyzed after 1 day and 112 days to assess the short- and long-term impact on the microstructure. To determine the porosity, 30 images with a resolution of 1280×960 pixels were captured over the entire surface of the sample with the same brightness and contrast. For each image, the porosity of the cement pastes was determined according to the shades of gray method using an arbitrary threshold according to Scrivener [30]. However, the value of the chosen threshold was determined in order to obtain a water/cement ratio of 0.5 on the cement reference sample according to the method proposed by Wong and Buenfeld [31]. The porosity of the cement paste was obtained by calculating the mean value on the 30 images.

2.2.7. Adsorption isotherm

In the adsorption test protocol outlined in the article, 200 mg of the carbon sample under examination was placed into a 50 mL tube, followed by the addition of 25 mL of the calcium solution. Calcium solutions of concentrations 25, 50, 100, 200, 300, 400, and 500 ppm were prepared using $CaCl_2$, and the pH was adjusted to 12.5 by adding a 100 g/L KOH solution. The tubes were agitated for 12 h in a tube rotator, then centrifuged at 5000 rpm for 15 min to separate the supernatant from the carbon particles. The recovered solution was filtered through a 0.2 μm syringe filter and diluted 10 times in a 5 % nitric acid solution. The diluted solutions were subsequently analyzed using an Agilent 5110 ICP-OES at 317.9 nm, with reference to a 1000 ppm calcium standard, to measure the residual calcium ion concentration. The method's limit of detection was 0.85 ppm, and the limit of quantification was 1.18 ppm.

3. Results and discussion

3.1. Rheology

The rheological properties were measured for each mix of cement/carbonaceous material paste. The results of the yield stress and plastic viscosity measurements obtained are presented in Fig. 2. The measurements of the various carbonaceous materials are compared to the results obtained for the Portland cement reference (red dotted lined). The different percentages of industrial graphite G1 showed values similar to the cement reference with stress yields and plastic viscosities respectively around 10 Pa and 0.07 Pa.s. For graphite G2, the replacement of 0.1 % to 2 % of cement allowed to observe an increase in yield stress and plastic viscosity clearly higher than G1. However, these increases

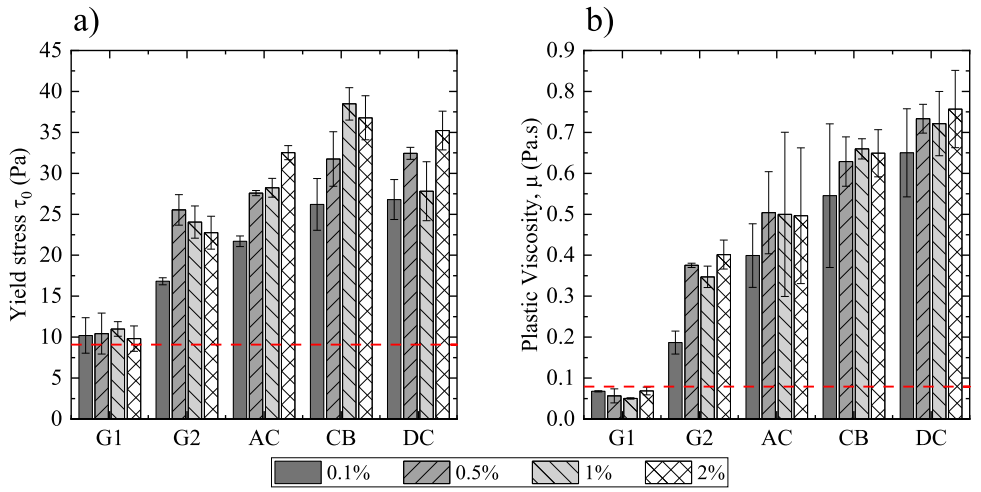

Fig. 2. Plastic viscosity and yield stress of cement and cement/carbon pastes. The red line refers to the cement reference paste.

stabilize respectively around 23 Pa and 0.35 Pa.s beyond 0.5 % replacement in G2. The increases of viscosity with the addition of natural graphite were also observed by Papanikolaou et al. [9]. The addition of activated carbon showed an increase in yield stress and plastic viscosity with the increase in the amount of AC. The same behavior was observed for black carbon CB and for the decolorized carbon DC with values three times higher compared to the cement reference for yield stress, and up to ten times higher for plastic viscosity. The yield stress and plastic viscosity results of graphite G1, carbon black CB and decolorized carbon were reported to result from an increase in surface area due to smaller particle sizes [32,33].

However, the results for G2 graphite and AC activated carbon are not consistent with the rest of the observations. These results seem to indicate that other parameters such as particle shape or particle porosity are responsible for these changes. Graphite G2 with its flake-shaped (Fig. A2) particles larger than graphite G1 showed higher yield stress and plastic viscosity values. Similarly, activated carbon with a higher porosity than G1 graphite showed higher yield stress and plastic viscosity results, despite a similar particle size. Moreover, the relatively close values between the decolorized carbon DC and the carbon black tend to show a partial dispersion of the carbon. Similar trends were observed by Abdulfattah et al. [34] on concrete slump tests. In general, apart for graphite G1, the addition of a small proportion of carbonaceous materials tends to increase yield stress and plastic viscosity. These results are consistent with observations made on several carbonaceous materials in cement that showed an increased water demand upon carbon addition [9,34,35]. However, apart from the particle size, due to the small percentage of replacement, it remains difficult to describe the effect of the type of carbon on the rheology of cement pastes.

3.2. Mortar compressive strength

The choice to conduct compressive strength and air void measurements on mortar samples rather than paste samples was made to better simulate real-world concrete applications, where the presence of aggregates significantly influences the mechanical and durability properties of the material [22,36]. Mortar samples, which include fine aggregates, provide a more accurate representation of the concrete's behavior under actual service conditions. The inclusion of aggregates affects the internal structure, air void distribution, and the overall response to mechanical stresses. Therefore, testing mortar samples allows for a more comprehensive understanding of how carbonaceous materials impact the performance of cementitious systems in practical applications. This approach ensures that the findings are directly applicable to the concrete used in the field, where the interaction between the cement paste and aggregates is crucial to the material's overall performance.

Fig. 3(a-e) respectively show the results of the relative compressive strength of the carbonaceous materials G1, G2, CA, CB, and CD as a function of time. The relative compressive strengths were calculated from the compressive strength results according to Eq. (4).

$$Relative\ strength = \frac{R^{j\ days}_{100\ cement} - R^{j\ days}_{\%\ carbon}}{R^{j\ days}_{100\ cement}} \quad (4)$$

where $R^{j\ days}_{100\ Cement}$ and $R^{j\ days}_{\%carbon}$ are respectively the compressive strength of the cement reference at j-days and the blended cement with carbonaceous materials at j-days, respectively. The compressive strength results are available in Fig. A5 in annex.

The addition of 0.1 % G1 graphite showed a slight increase in compressive strength, especially at 1 day. However, increasing up to 2 % the cement replacement for G1 graphite generally showed a decrease of about 5–10 % in compressive strength. Similar results were observed by Luo and Wang [37] and Wu et al. [10]. In addition, the manufacture of industrial graphite is carried out from the cooking of coke, which suggests that graphite G1 is partly composed of amorphous uncooked coke residues. The study of Justo-Reinoso et al. [16] showed a decrease in compressive strength with the addition of coke in the cement, which tends to confirm the observations. For G2 natural graphite, a strong increase in compressive strength of 20 to 40 % was observed at 1 day for the different replacement levels. However, after 7 days and more, the observed strengths remain similar to the cement reference. Same tendencies to G2 graphite were reported in other articles [9,6,7,38] where commercial activated carbon showed a strong increase in compressive strength at 1 day, specifically for blends with 0.1 % and 0.5 % AC. On the other hand, this increase was less visible for the mixes with 1 % and 2 % AC. In their study, [17] observed similar results for activated charcoal replacement of 1 % and 2 %. In general, the compressive strengths beyond 7 days showed slightly better results for AC than the cement reference. This difference can be due to the presence of about 7 % of quartz in AC, which is weakly reactive. For decolorized carbon DC, results similar to activated carbon were observed, showing higher compressive strengths at 1 day than the cement reference. However, beyond 1 day, the compressive strength of the DC mortar showed a similar result to that of the AC mortar. These results seem to confirm that the presence of quartz in AC had no improvement on the AC mortar compressive strength for these replacement levels. For carbon black CB, results similar to DC were observed with an increase in compressive strength at 1 day and values similar to the reference after 7 days. However, replacing the cement with 2 % CB showed a decrease in

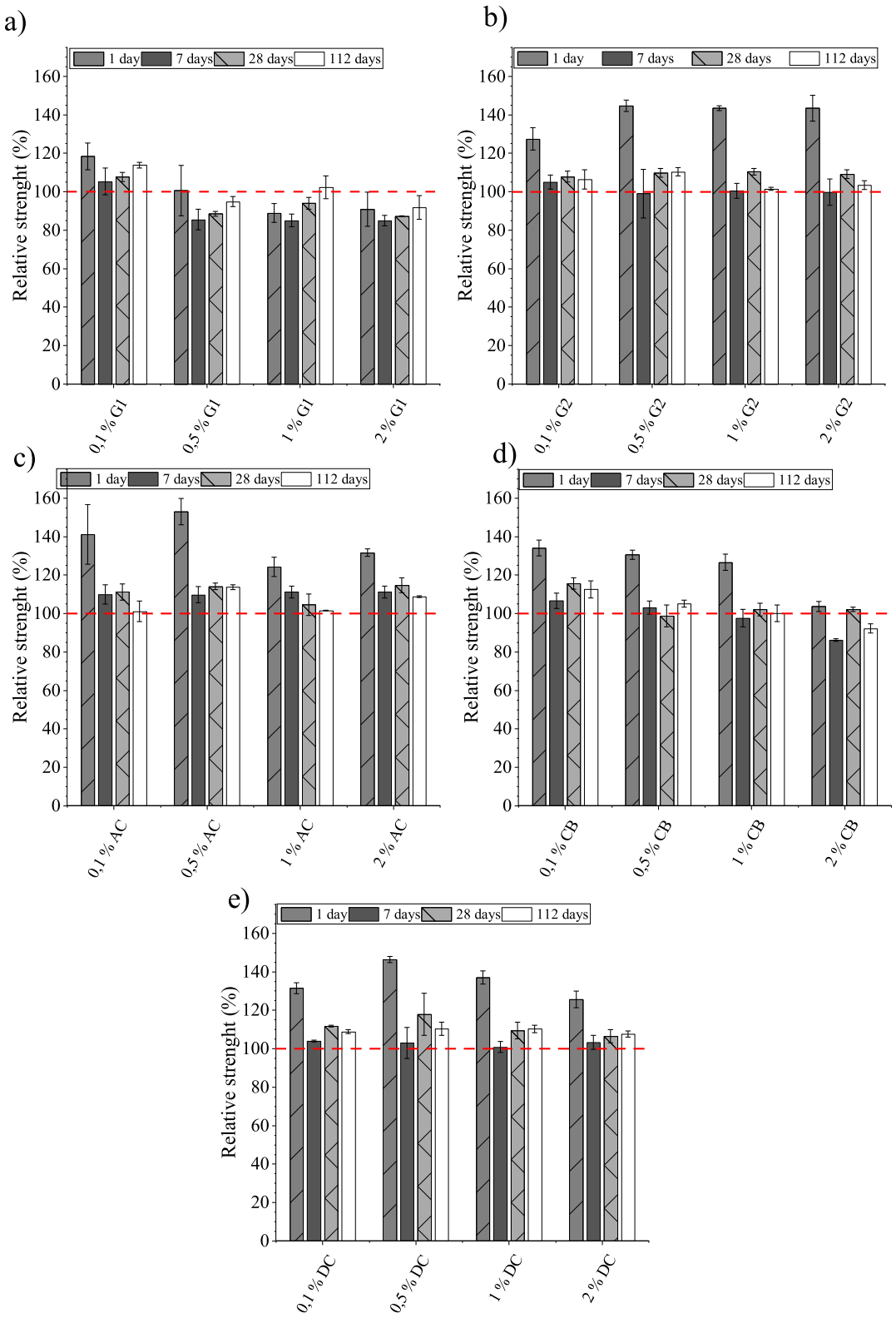

Fig. 3. Relative compressive strength of mortar samples a) graphite G1, b) graphite G2, c) Activated charcoal AC, d) carbon black CB, e) decolorized charcoal DC at 1, 7, 28 and 112 days. The red line refers to the cement reference mortar sample.

compressive strength beyond 7 days. These results are contradictory to the observations made by Abdulfattah et al. [34] where compressive strength gains were maintained over time despite adding carbon black. This contradiction from the results in the present study seems to confirm the hypothesis of poor dispersion of CB during the mixing process.

In general, apart from G1 graphite, the addition of carbonaceous materials shows a setting accelerator effect with an increase in the compressive strength at 1 day. However, beyond 7 days, the compressive strengths no longer seem to be affected by the presence of a small proportion (2 % and less) of carbon. However, the crystallinity, or the

size of the carbon particles, therefore, does not seem to explain the accelerator effect. In addition, questions remain on the effect of using superplasticizer in order to maintain a constant flow in accordance with ASTM C109. Indeed, the reference and the G1 graphite mixes did not require the addition of superplasticizer as there was no increase in the water demand. However, the dispersion of carbon particles is a parameter that significantly influences the properties of cementitious materials. This is why, apart from the tests on mortar, the other characterization tests were carried out without using a superplasticizer.

3.3. Air in hardened mortar

Fig. 4a presents the results of air void measurements in the hardened state of mortars with different proportions of carbonaceous materials. The G1 graphite showed air values 2 % to 4 % higher than the cement reference. This strong increase in the quantity of air can explain the lower compressive strengths observed. The other carbonaceous materials also showed around 2 % increases in the amount of air, which remains lower than the G1 graphite. The two types of graphite, on the other hand, entrain a greater quantity of air. In addition, the AC activated carbon showed similar amounts of air to the cement reference, which supports the improved long-term compressive strength results than the reference.

However, these observations cannot clearly define a trend between the replacement levels and the quantity of air observed. Fig. 4b plots the quantity of air at 28 days versus the compressive strengths for the different days tested. As shown in Fig. 4b, the results do not show a strong correlation between the compressive strength measurements and the amount of air. However, the equations showed similar trends to observations made by Pinto and Hover [39] with an 3 % decrease in compressive strength per percentage of air added. This high variability may be explained by the measurement method in the hardened state done by image analysis. Indeed, since the mortar samples were made with Ottawa sand its smaller grain size of sand may be more easily teared apart. However, the image analysis method cannot differentiate an air void from a void left by the tearing of an aggregate. This effect is visible in Fig. A3 in the Appendix. The tearing of the aggregates is also linked to the resistance of the cement paste. It is therefore possible that the results are slightly overestimated for mortars with the least resistant cement pastes such as G1 graphite.

3.4. Thermogravimetric analysis

Samples with 2 % replacements were tested by TGA at 1 day, 28 days, and 112 days. Figs. 5-7 show the relative masses of the DTGs from the various carbonaceous materials tested respectively at 1 day, 28 days, and 112 days. At 1 day the samples containing graphite G1 and carbon black showed similar results to the cement reference, with relatively similar mass losses between 30 °C and 500 °C. These results suggest that the samples precipitated similar amounts of hydrates. On the other hand, the samples containing activated carbon AC, natural graphite G1, and decolorized carbon DC showed greater mass losses than the other samples between 30 °C and 500 °C. These differences are particularly visible between 30 °C and 300 °C which are the temperatures associated with C-S-H, ettringite (AFt) and monosulfates/monocarbonate (AFm) [29]. These results indicate greater hydrate precipitation for these mixes. However, it remains difficult from the TGA data to identify precisely which phase was most influenced by the presence of carbonaceous materials.

Other differences are observable from 600 °C and above. Activated carbon AC and decolorized carbon DC showed a higher proportion of calcite. These results seem consistent with AC activated carbon due to

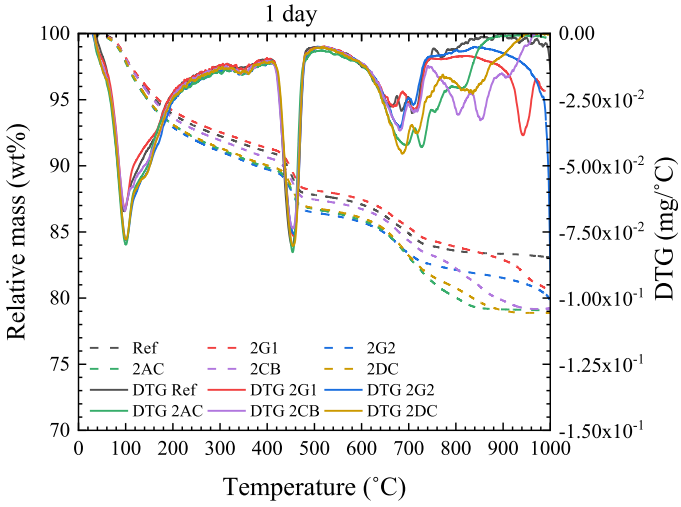

Fig. 5. TG and DTG curves of cement and cement/carbon pastes samples at 1 day.

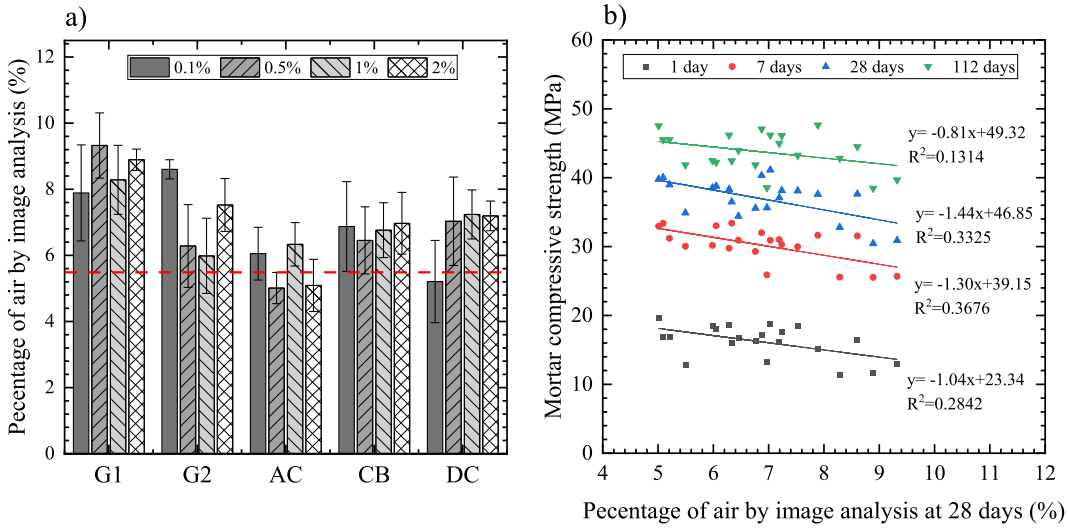

Fig. 4. a) Percentage of air in mortar at 28 days measure by the image analysis and b) air percentage at 28 days versus the compressive strength. The red line refers to the cement reference mortar sample air content.

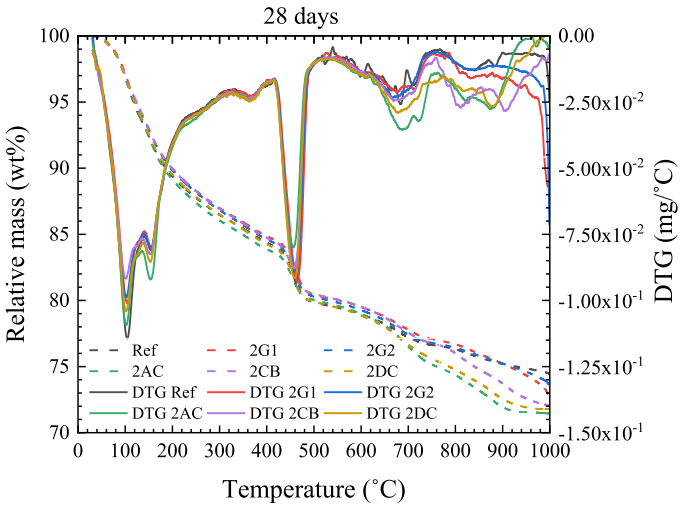

Fig. 6. TG and DTG curves of cement and cement/carbon pastes samples at 28 days.

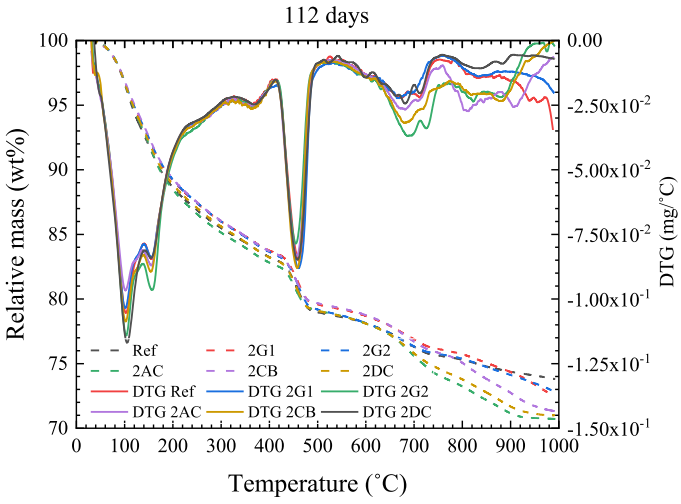

Fig. 7. TG and DTG curves of cement and cement/carbon pastes samples at 112 days.

the presence of calcite in this commercial activated carbon. However, the decolorized carbon DC does not contain calcite. These observations leave two possible hypotheses: carbonation of the sample or carbon oxidation from DC. Since the structure of decolorized carbon is similar to that of activated carbon, and the amounts of portlandite are similar in the two samples, the oxidation hypothesis seems more consistent. Mass losses above 750 °C are due to the oxidation of different carbonaceous materials, which explains the different temperatures observed. At 28 days, similar mass losses are observable for all the carbonaceous materials and the reference. However, activated carbon AC and decolorized carbon DC seem to show a slightly higher presence of AFm. The main notable differences are visible above 600 °C with a greater presence of calcite for the activated carbon and different oxidation temperatures of the carbonaceous materials. At 112 days, results similar to those at 28 days are observed. However, greater mass losses between 60 °C and 400 °C are observed, indicating a more significant formation of hydrates over time. Nonetheless, no significant differences are observed for the other phases.

From the TGA data at 1 day, 28 days and 112 days, it is possible to estimate the degree of hydration of the cement paste according to the method proposed by Monteagudo et al. [40]. However, that study showed that the amount of water bound for an infinite hydration time is dependent on the additions of SCM made to the cement. This is why, in this study, the bound water mass for infinite hydration times was characterized by regression of the bound water masses measured at 1 day, 28 days and 112 days according to the method proposed by Monteagudo et al. [40]. The results on the evolution of the degree of hydration over time are presented in Fig. 8a. At 1 day, graphite G1 shows a degree of hydration similar to the reference. On the other hand, the other carbonaceous materials showed slightly higher degrees of hydration of 6 % to 8 % compared to the reference. At 28 days and 112 days, all the carbonaceous materials seem to show equivalent degrees of hydration or slightly lower by 1 % to 4 % compared to the reference. Like the results at 1 day, these results confirm the trends observed on mortars with an accelerating effect at 1 day, but which is no longer observable after 7 days.

In addition, the very low concentrations of silica and aluminum in the carbons tested suggest that the precipitation of a greater amount of hydrate is not due to chemical reactions with the carbon. The increase in the quantity of hydrates and the degree of hydration would rather be due to chemisorption phenomena, allowing better nucleation of the hydrates.

From the TGA data, it is also possible to describe the microstructure of the dough according to the method proposed by Adu-Amankwah et al. [41]. This method allows to estimate the porosity from the measurement of the bound water mass measured by TGA, and by assuming that the average density of the bound water is 1.3 g/cm^3 [42]. Fig. 10b shows the evolution of the porosity composition calculated by TGA as a function of time. The mixture with 2 % of graphite G1 at 1 day showed a porosity similar to the reference around 51 %. On the other hand, slightly lower porosities around 50 % were observed for the other carbonaceous materials.

However, as for the degree of hydration, all the mixes showed porosities similar to the reference with values respectively 42 % and 39 % at 28 days and 112 days. These results tend to explain the greater compressive strengths observed on mortars at 1 day, and similarly beyond 28 days. Nevertheless, the porosity calculation method cannot estimate the real porosity due to its sensitivity to carbonation and the density assumption made for bound water density.

3.5. *BSE scanning electron microscopy*

Porosity measurement was also based on scanning electron microscopy observations. These measurements were intended to confirm the porosity trends calculated from the TGA observations. Fig. 9a presents the porosity results of the cement pastes at 1 day and 112 days calculated from the shades of gray of 30 images. As for the measurement of porosity by TGA, the measurement of porosity by SEM does not provide the real porosity of the paste, but a trend [29]. Real porosity cannot be obtained, because the threshold for calculating porosity from shades of gray is taken arbitrarily [30]. At 1 day, the reference showed approximately 43 % porosity. A slightly higher porosity of 43.8 % was observed for the sample containing the G1 graphite. The samples containing carbon black DC and the decolorized carbon allowed to obtain porosities slightly lower than the reference around 42 %. Finally, natural graphite G2 and activated carbon AC showed slightly lower porosities around 41 %. Similar results were observed by Justo-Reinoso et al. [17] for the activated charcoal. At 112 days, porosities greater than the reference were observed for graphite G1 and carbon black with respective values of 29.7 % and 28.7 %. The other carbonaceous materials showed smaller differences compared to the reference, with porosities around 27.5 % against 28 % for the reference.

Fig. 9b shows the relationships between the compressive strength and the different porosity measurements performed by TGA and SEM. Unlike the observations made by TGA, the porosity measurements by SEM showed slightly larger differences between the different samples. This difference can be explained by the greater quantity of samples analyzed (30 images for the SEM against 3 samples for the TGA

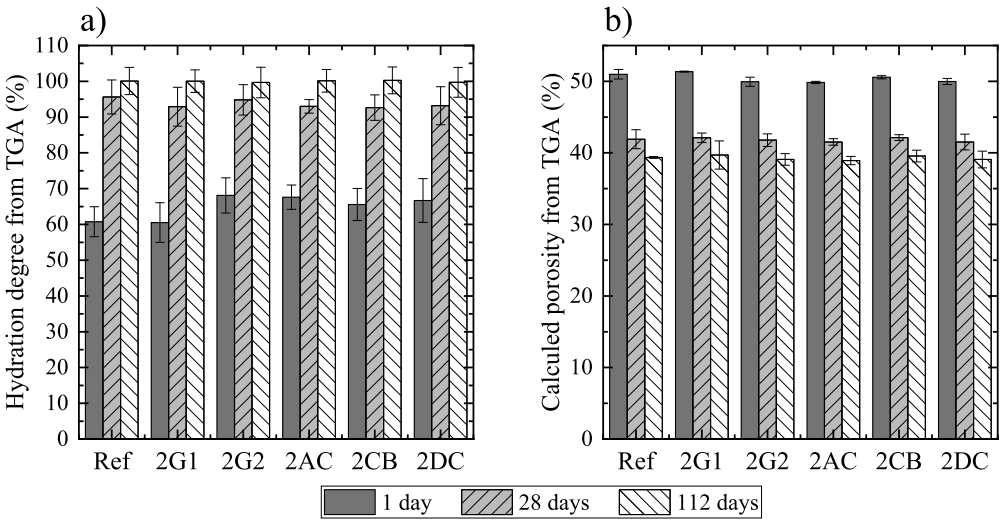

Fig. 8. a) Hydration degree and b) porosity calculated from TGA results at 1, 28 and 112 days.

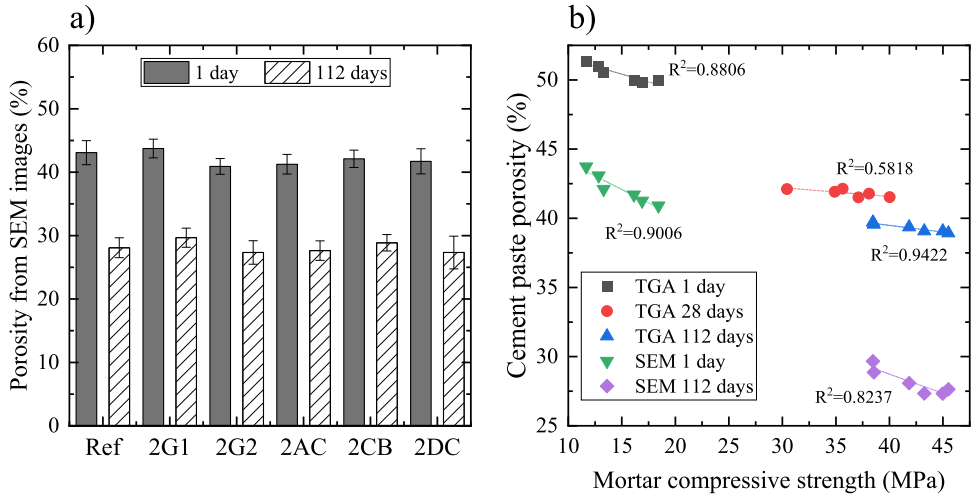

Fig. 9. a) Porosity measured form SEM images and b) cement paste porosity obtained by SEM and TGA versus mortar compressive strength.

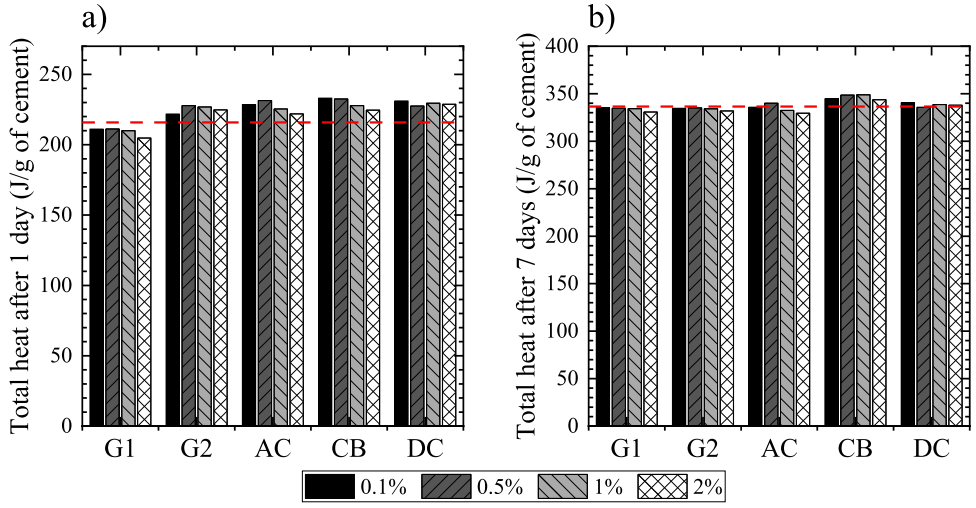

Fig. 10. Total heat released measure by isothermal calorimetry after a) 1 day and b) 7 days. The red line refers to the cement reference mortar sample.

measurements). Moreover, unlike TGA tests, which are based on assumptions, SEM measurement of porosity is based on direct observation of porosity.

The compressive strength measurements of mortars are correlated to the porosity of cement pastes. The addition of carbonaceous materials, apart from industrial graphite, seems to reduce the porosity at a young age. However, the differences in porosity are less noticeable beyond 28 days, which explains the same compressive strength results at 112 days. Moreover, for G1 graphite, the increase in porosity can be explained by the greater presence of air in the paste.

3.6. Isothermal calorimetry

The cement/carbonaceous material mixes were analyzed by isothermal calorimetry. The results of the heat fluxes measured for the different paste samples are presented in Fig. A4 in the Appendix. From the integral of the heat flux, it is possible to measure the total heat released for cement/carbonaceous material pastes. Figs. 10(a and b) respectively present the results of heat released at 1 day and 7 days for the various materials tested with replacements of 0.1 %, 0.5 %, 1 % and 2 %. At 1 day, the G1 graphite showed slightly less heat release, about 2.3 % to 4.6 % less, than the reference. This decrease in the amount of heat is accentuated by greater levels of G1 graphite replacement. For the other carbonaceous materials, greater heat releases are observed with increases of 3 % to 8 % depending on the carbon. Apart from decolorized carbon DC, the increase in the amount of heat depends on the level of carbon replacement. For carbon black CB, a decrease in heat release is observed when the quantity of CB increases. On the other hand, for graphite G2 and activated carbon AC, a maximum release is observed for replacements at 0.5 %. At 7 days, the observed heat releases are similar to the reference release. Only carbon black showed a slightly higher heat release, higher by 2 % to 5 %, compared to the reference at 7 days. These results indicate a greater amount of chemical reaction at 1 day for the G2, AC, CB, and DC carbons. Graphite G1, on the other hand, showed a lower amount of chemical reactions. However, at 7 days, the amounts of heat remain similar for the different carbons. These results confirm the trends observed by TGA and seem to indicate an accelerating effect.

On the other hand, except for graphite G1, reductions in the final setting time are observed for the other carbonaceous materials (G2, AC, CB, and DC). Industrial graphite G1 mix showed an increase in final setting time with the addition of G1. Nevertheless, these final set values remain in the same trend to the cement reference. The main hypothesis to supports the delays in initial setting time enforce that the ions available in the solution are captured at the surface of the carbon grains, which would slow down the onset of hydration. On the other hand, the deposition of ions on the surface of the carbon grains could possibly turn the carbon grains into nucleation points that would accelerate the precipitation of hydrates and to reduce the final setting time. Finally, this explains the greater release of heat at 1 day.

From the first derivative of the heat flow curves, it is possible using the method proposed by Hu, Ge and Wang [43] to estimate trends in the initial and final setting times of the dough. Fig. 11(a and b) present respectively the initial and final setting times calculated from the calorimetry curves. All the carbons showed longer initial setting times than the cement reference. For graphite G1, activated carbon AC and carbon black, increases in initial setting time appears, with delay increasing from 15 min to 50 min, with increasing carbon replacement. Graphite G2 showed a decrease in initial setting time delay, decreasing from 20 min to 15 min with increasing addition of G2. The decolorized charcoal showed an initial set delay of approximately 25 min for the different levels of replacement.

The method proposed by Berodier and Scrivener [44] can be used to characterize the acceleration of hydration reactions by measuring the slope of the heat flux curves during the acceleration period. Fig. 12a shows the slopes of the heat flow curves for the different carbonaceous materials tested with replacements of 0.1 %, 0.5 %, 1 %, and 2 %. For graphite G1, slopes similar to the cement reference are observed. G2 graphite and AC activated carbon showed the largest slope increases, around 43 %. The decolorized carbon also showed a slope increase of 32 %. On the other hand, for carbon black, a lower increase, of around 20 %, was observed.

As shown in Fig. 12b, the slope values of the heat flow in the accelerating period were correlated with the measurements of porosity and compressive strength at 1 day for samples containing 2 % carbon to understand their effect on each other. The results showed good correlations between the porosity measured at 1 day by TGA and SEM with the slope values. These results show that the acceleration of the setting is responsible for the decrease in the porosity of the dough. However, the porosity values were directly correlated to the compressive strengths as a correlation of the slope values with the compressive strengths at 1 day is also observable.

3.7. Calcium adsorption isotherm

This study employed an extensive array of isotherm adsorption models to predict different adsorption phenomena. These predictions were based on the equilibrium concentration of the adsorbate and the mass of the calcium adsorbed at equilibrium. The models utilized included Freundlich, Langmuir, Temkin, and Dubinin-Radushkevich models.

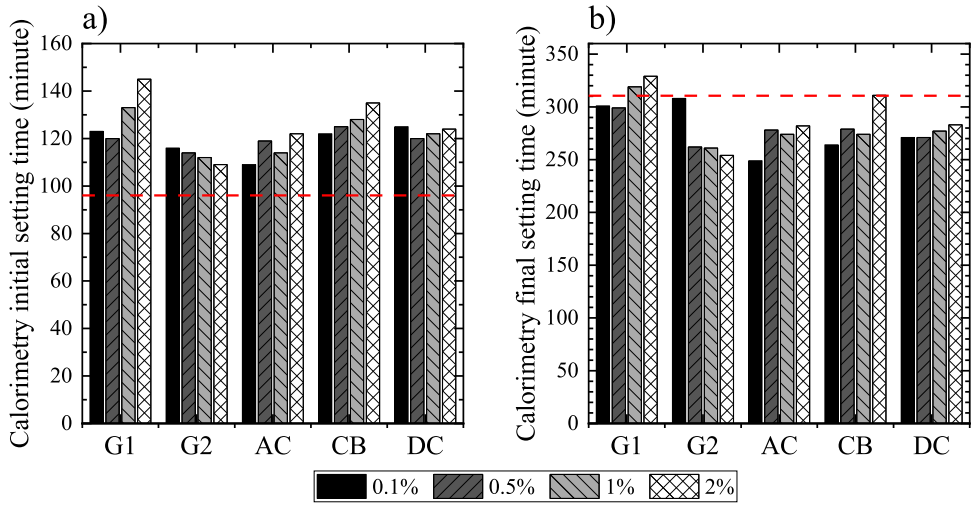

Fig. 11. a) Initial and b) final setting time measure by isothermal calorimetry. The red line refers to the cement reference mortar sample.

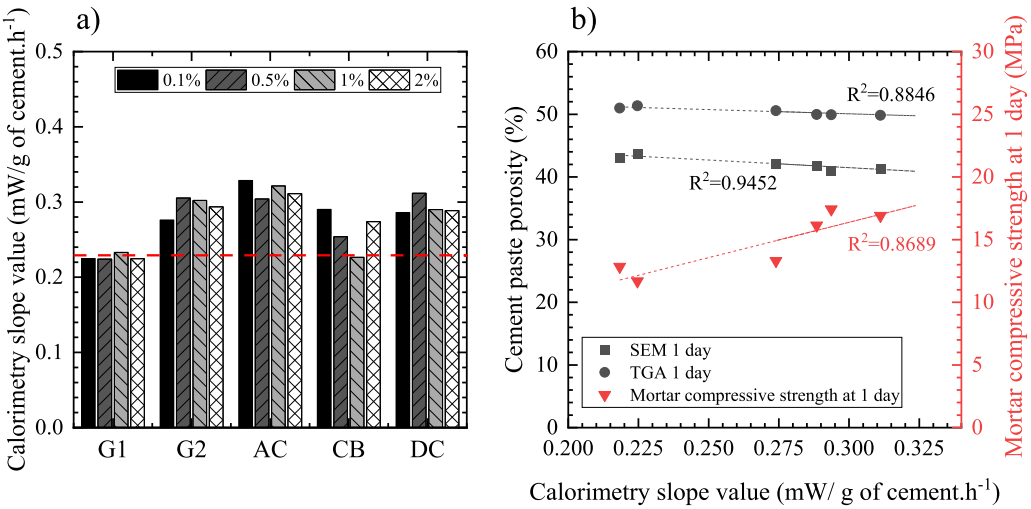

Fig. 12. a) Calorimetry slope value of cement and cement/carbon pastes. b) Calorimetry slope value on cement paste versus cement paste porosity and mortar compressive strength. The red line refers to the cement reference mortar sample.

The Freundlich isotherm adsorption model examines how adsorption occurs on uneven surfaces and considers the interactions between the adsorbed molecules [45]. It allows for multilayer adsorption and indicates that the adsorption energy decreases as the adsorption process continues within the adsorbent. Mathematically, it is expressed as [45–47]:

$$Q_e = K_F C_e^{1/n} \tag{5}$$

Here, K_F represents the Freundlich constant, while C_e denotes the equilibrium concentration of the adsorbate (mg/L). The parameter n signifies the non-linear degree, delineating various adsorption processes. The reciprocal $1/n$ provides additional insights into the adsorption process: $1/n\langle 1$ signifies normal adsorption, $1/n\rangle 1$ indicates non favorable adsorption [46].

The Langmuir isotherm model posits monolayer adsorption on homogeneous surfaces, without interactions among adsorbed molecules [45]. It suggests that the formation of a monolayer adsorbate hinders further adsorption, as expressed by the equation [45–47]:

$$Q_e = \frac{K_L Q_{max} C_e}{1 + K_L C_e} \tag{6}$$

Here, K_L and Q_{max} represent the Langmuir adsorption constant and the monolayer adsorption capacity (mg g^{-1}), respectively [46].

The Temkin model explicitly considers interactions between the adsorbent and adsorbate, depicting the heat of adsorption as a function of temperature [45–47]:

$$Q_e = \beta_T \ln(C_e) + \beta_T \ln(A_T) \tag{7}$$

Where A_T represents the equilibrium binding constant, and β_T represents the Temkin isotherm constant.

Conversely, the Dubinin–Radushkevich isotherm articulates the adsorption mechanism, featuring a Gaussian energy distribution on a heterogeneous surface [45–47]:

$$\ln(C_e) = \ln(Q_{max}) - \beta\left(RT\ln\left(1 + \frac{1}{C_e}\right)\right)^2 \tag{8}$$

Here, Q_{max}, and β, represent the theoretical isotherm saturation capacity and the Dubinin-Radushkevich theoretical isotherm saturation capacity, respectively. Here, T is the absolute temperature in kelvin, and R is the Boltzmann gas constant (8.314 J/mol K). The Gaussian energy distribution on the heterogenous surface can be described with the following equation:

$$E = \frac{1}{\sqrt{2\beta}} \tag{9}$$

E is the energy, describing the adsorption potential [48]:

If E ⟨ 8 kJ/mol is chemisorption, and E ⟩ 8 kJ/mol is physisorption

The results from the isotherm adsorption experiments on various carbonaceous materials using different models reveal insights into the adsorption mechanisms and behaviors of these materials. These results are presented in Table 4.

For G1, the Dubinin–Radushkevich (DR) isotherm model shows an E value indicating chemisorption. The Langmuir isotherm model fits the data best with an R^2 value of 0.945, compared to the Freundlich and Temkin models. This supports the hypothesis that surface chemistry plays a more critical role in the adsorption and accelerating effects observed in carbon particles than particle size or mineralogy. G2 exhibits higher adsorption capacities compared to G1. The DR model suggests chemisorption. The Langmuir model again fits best with a high R^2 value of 0.987, outperforming the Freundlich and Temkin models. This reinforces the importance of surface chemistry in determining adsorption behavior.

For material AC, the DR model indicates physisorption with a higher E value. Despite the higher Qmax value from the Langmuir model, the

Table 4
List of calculated parameters from the Dubinin–Radushkevich, Langmuir, Freundlich, and Temkin adsorption isotherm models.

	Carbonaceous materials				
Isotherm	G1	G2	AC	CB	DC
Dubinin–Radushkevich					
β (mol^2/kJ^2)	0.0087	0.0090	0.0032	0.0082	0.0027
Q_{max} (mol g^{-1})	0.0453	0.1849	0.2102	0.1091	0.1865
E (kJ/mol)	7.5636	7.4358	12.4462	7.8222	13.5433
R^2	0.9504	0.9771	0.9435	0.9576	0.9777
Langmuir					
Q_{max} (mg g^{-1})	0.9641	3.8003	5.6469	2.2585	5.1575
K_L (L/mg)	0.0041	0.0041	0.0433	0.0054	0.0742
R^2	0.9449	0.9874	0.8349	0.9780	0.8300
Freundlich					
K_F (L/mg)	0.0205	0.0740	1.3522	0.0669	1.5894
n	1.7740	1.7305	4.1615	1.9060	4.9152
R^2	0.9479	0.9623	0.9619	0.9348	0.9927
Temkin	0.0000	0.0000	0.0000	0.0000	0.0000
A_T (L/g)	0.0543	0.0516	1.6424	0.0536	2.8108
β_T	0.1902	0.7564	0.8468	0.5011	0.7479
b (kJ/mol)	12.8079	3.2203	2.8766	4.8609	3.2573
R^2	0.9355	0.8648	0.7736	0.8500	0.7964

Freundlich model is a better fit due to its higher R^2 value of 0.962. This suggests that surface heterogeneity is a significant factor in adsorption processes for this material, further supporting the emphasis on surface chemistry over other factors. CB exhibits moderate adsorption capacities with the DR model indicating chemisorption. The Langmuir model is most appropriate here with the highest R^2 value of 0.978. This again underscores the critical role of surface chemistry in adsorption phenomena. DC shows high adsorption capacities, with the DR model indicating physisorption. Despite a lower Qmax value, the Freundlich model is the most suitable, given its exceptionally high R^2 value of 0.993. This suggests that surface heterogeneity and interaction energies are pivotal, highlighting the overriding influence of surface chemistry.

In this study, the Langmuir, Freundlich, and DR models are the most appropriate for describing the adsorption behavior of the materials studied, depending on their specific characteristics and experimental data.

3.8. Mechanism of carbonaceous materials on cement hydration

The impact of carbonaceous materials on the hydration of Portland cement was studied with the compressive strength of mortar, TGA, SEM, isothermal calorimetry and isotherm adsorption tests. Based on these results, it is possible to understand at the fresh and hardened the mechanism of carbonaceous material on cement hydration. In the fresh state, the impact of the addition of carbonaceous materials on the rheological properties will vary depending on the size, shape and dispersion of the grains. If their size and shapes are similar to cement grains, the addition of carbon will have little impact on rheology. On the other hand, carbon particles of smaller size or of more angular shape will lead to an increase in all rheological parameters. Moreover, since the quality of the dispersion affects the real size of the particles, it is intuitive to think that a bad dispersion will decrease the yield stress and the viscosity of a mix due to larger agglomerated particles. The presence of carbon will also lead to changes in the hydration of the cement.

Fig. 13 presents a comparative analysis of the maximum adsorption capacities calculated using the Dubinin-Radushkevich and Langmuir models, plotted against the calorimetry slope value. Black squares in the plot indicate the Q_{max} values derived from the Dubinin-Radushkevich model. These values show a strong positive correlation with the calorimetry slope value, as evidenced by the fitted dashed black trend line with an R^2 value of 0.9139. This high R^2 value signifies a robust linear relationship between the calorimetry slope and the adsorption capacity according to the Dubinin-Radushkevich model. In contrast, red squares represent Q_{max} values calculated using the Langmuir model. The corresponding dashed red trend line, which has an R^2 value of 0.7648, also indicates a positive correlation with the calorimetry slope value. However, the lower R^2 value compared to the Dubinin-Radushkevich model suggests a relatively weaker linear relationship.

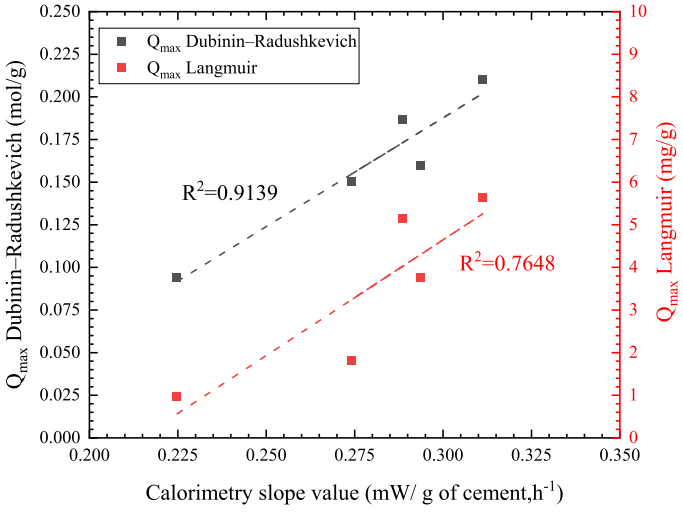

Fig. 13. Calorimetry slope values vs theorical maximum Calcium adsoprtion for DR and Langmuir isotherm models.

The calorimetry slope values are linked to the filler effect and the acceleration effect. These results confirm the trends between the adsorption of calcium on the surface of the carbon grain and the accelerating effect. They tend to confirm the greater importance of surface chemistry over particle size or the mineralogy of the carbon particles. While several results in the literature already show that for one type of carbon, the finer the material, the more significant the effect on hydration will be, for different carbon materials, the surface chemistry is more crucial.

This figure demonstrates that both the Dubinin-Radushkevich and Langmuir models exhibit a positive correlation between the calorimetry slope value and the maximum adsorption capacity. With the Dubinin-Radushkevich model showing a stronger correlation with an energy value <8 kJ/mol in most cases. The DR isotherm model, characterized by its ability to describe adsorption processes onto porous surfaces with heterogeneous energy distributions, indicates the nature of adsorption through its mean free energy parameter [45–47]. When E is <8 kJ/mol, chemisorption is indicated. This supports the hypothesis that surface chemistry plays a more critical role in the adsorption and accelerating effects observed in carbon particles than particle size or mineralogy.

Fig. 14 schematically illustrates the impact of carbon on hydration and microstructure. In the initial state, the carbon particles only influence the rheological properties as explained above. In addition, certain carbons, such as industrial graphite G1, showed greater air entrainment in the paste. However, as shown by the calorimetry data, the initial setting of the cement will be delayed as ions in solution are captured by the chemisorption phenomenon on the surface of the carbon grains. This phenomenon does not depend on the crystallinity, the type of carbon, or the size of the particles. This suggests that the initial setting is influenced by surface properties and carbon chemisorption. The deposition of ions from the solution on the grains will thus promote the nucleation of hydrates on the surfaces of the carbon grains. In doing so, the increase in nucleation will lead to a greater precipitation of hydrates at 1 day, which will, in turn, accelerate the hydration of the cement. The formation of hydrates around the carbon grains will allow the formation of greater bonds in the cementitious matrix, which will affect the microstructure by reducing the porosity. This reduction will result in an increased compressive strength at 1 day. However, simultaneously, the increased presence of air entrained in the microstructure will conversely lead to a decrease in porosity. This increase will result in a decrease in mechanical properties. This is significantly observed with industrial graphite G1.

In the long term, since the carbon grains are not reactive, their effects on hydration are limited. For small amounts of carbon replacement (less than or equal to 2 %), their differences in porosity compared to the reference will decrease over the long term, which is probably due to the carbon grains being totally covered in hydrates and thus, may not provide additional nucleation sites. The results on mechanical performance also tend to confirm the previous. On the other hand, as shown in other studies [9,16,17], the addition of higher proportions of carbon will, conversely, lead to an embrittlement of the microstructure and negatively impact the mechanical properties. This observation can also be explained through the same mechanism. With a higher carbon content, more ions in solution were absorbed which created a delay in hydration as observed by Dutta, Bordoloi and Borthakur [16] leading to an increased porosity and decreased mechanical properties as shown by Justo-Reinoso et al. [17]. Qu et al. [13] also observed on carbon spots in cement, which suggests that this mechanism may extend to carbon-based nanomaterials such as graphene or graphene oxide.

The utilization of carbonaceous materials in cementitious systems, despite the modest benefits observed, can be of significant interest for specific applications. These materials are often explored for their ability to enhance certain functional properties of concrete, such as electrical

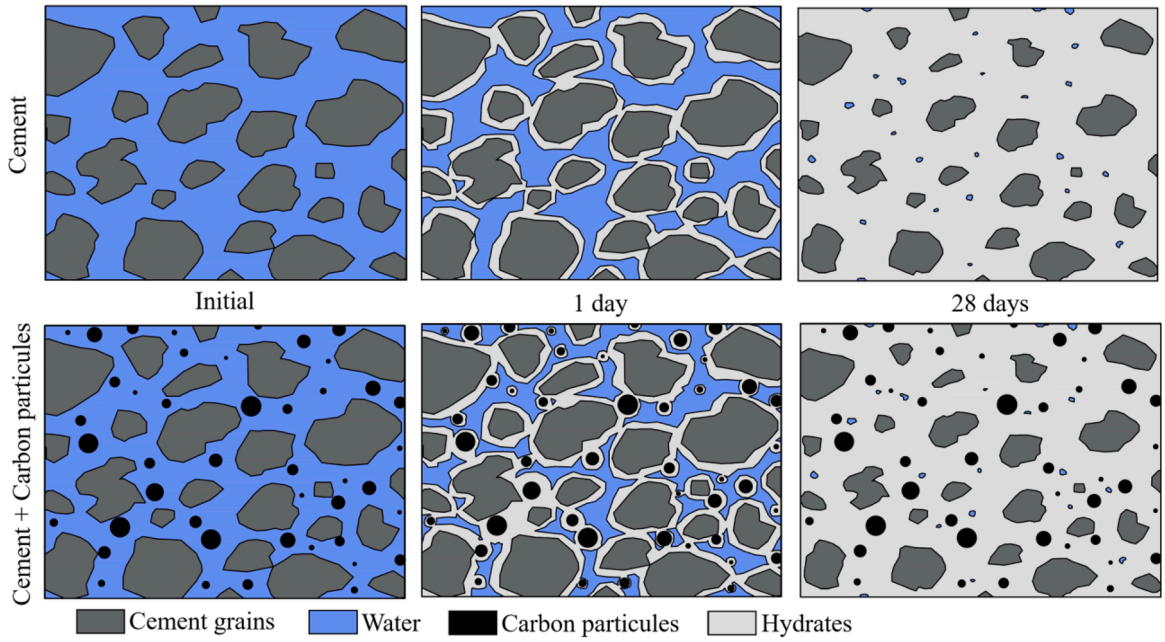

Fig. 14. Schematic representation of carbon particles effect on cement hydration.

conductivity [37], which are critical in advanced construction technologies. Although the direct impact of these materials on hydration and mechanical properties might appear limited, especially at low dosages, they play a crucial role in influencing the microstructure and early-age performance of the concrete. Additionally, in cases where unintentional contamination by carbonaceous materials might occur—such as through impurities in supplementary cementitious materials (SCMs)—understanding their effects becomes essential for ensuring the quality and reliability of the concrete. Thus, the investigation of carbonaceous materials at low dosages provides valuable insights into optimizing their use and mitigating potential adverse effects in practical applications.

4. Conclusion

This study investigated the effect of adding carbonaceous materials at low dosage on cement hydration through different techniques such as compressive strength mortar, TGA, SEM, isothermal calorimetry and rheology. These tests studied the influence of carbonaceous materials' properties on cement hydration. Based on the results presented, the following concluding remarks are drawn:

a. Carbon addition generally increases the water demand of cementitious materials. These increases were characterized through an increase of yield stress and plastic viscosity due to different parameters such as particle size, particle shape, and level of dispersion dictate the level of water demand.
b. The presence of carbonaceous materials showed greater air entrainment in the mortars by 2 %. However, G1 industrial graphite showed greater air entrainment with increases of up to 4 %. In this study, it was not possible to correlate the increases in the amount of air to the proportions of carbon replacement. In addition, the precise cause of this increase in the amount of air remains undetermined at the moment.
c. With the exception of industrial graphite G1, the various carbonaceous materials showed an acceleration of setting after 1 day by favoring the nucleation of hydrates which reduces the porosity and improves the mechanical properties. On the other hand, traces of this acceleration are no longer visible beyond 28 days.
d. The accelerating effect of carbons appears to be independent from crystallinity, mineralogy, or particle size, but rather on surface chemistry and quality of particle dispersion.
e. The accelerating effect of carbons was more significant for activated carbon AC, decolorized carbon DC, and natural graphite G2. Carbon black showed a significant acceleration of hydration for replacement levels lower or equal to 0.5 %. However, the accelerator effect was not observed on industrial graphite G1 or on carbon black, with a 2 % replacement.
f. In the calcium adsorption tests, both the Dubinin-Radushkevich and Langmuir adsorption models display a positive correlation between the calorimetry slope value and the maximum adsorption capacity. The Dubinin-Radushkevich model, however, shows a stronger correlation. This finding supports the hypothesis that surface chemistry is more critical in influencing the adsorption and accelerating effects in carbon particles than particle size or mineralogy.

CRediT authorship contribution statement

Victor Brial: Writing – review & editing, Writing – original draft, Visualization, Validation, Software, Methodology, Investigation, Formal analysis, Data curation. **Thomas Duplessis:** Investigation. **Claudiane M. Ouellet-Plamondon:** Writing – review & editing, Supervision, Software, Resources, Project administration, Methodology, Investigation, Funding acquisition, Data curation, Conceptualization.

Declaration of competing interest

The authors declare that they have no known competing financial interests or personal relationships that could have appeared to influence the work reported in this paper.

Data availability

Data will be made available on request.

Acknowledgments

The authors are grateful to the NSERC CRD grant program (CRDPJ

515485–17), CRITM consortium, Rio Tinto and Ciment Québec Inc. for their financial support of the start of this project, as well as the Canada Research Chair Program (CRC-2019–00074) for completing the study.

Appendix

Figs. A1, A2, A3, A4, A4, A5, A6

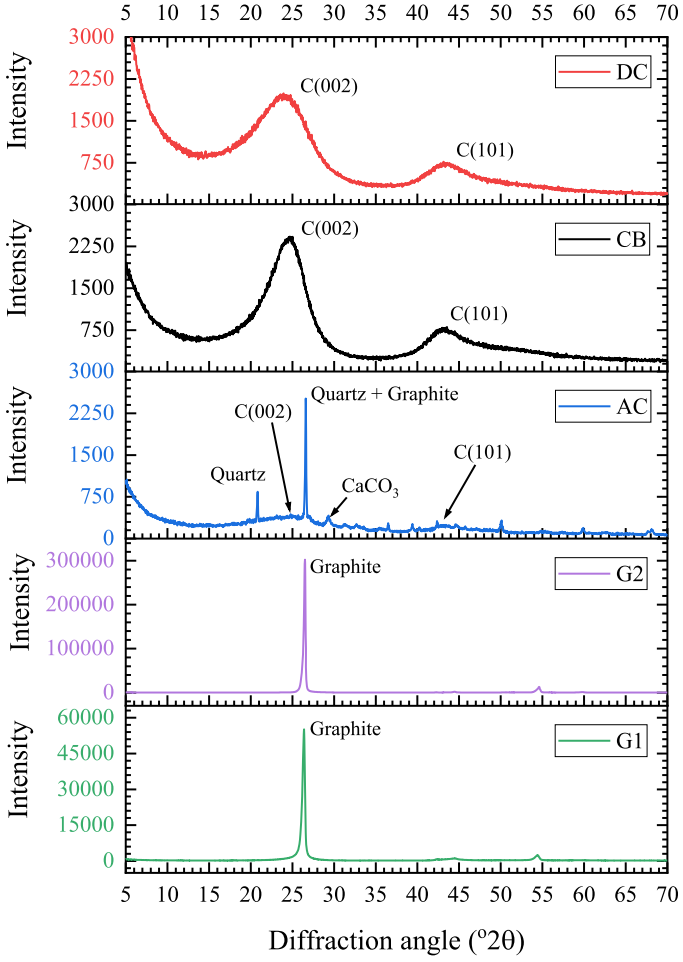

Fig. A1. XRD patterns of carbonaceous materials tested. The y axis scale has different scale for graphite G1 and G2.

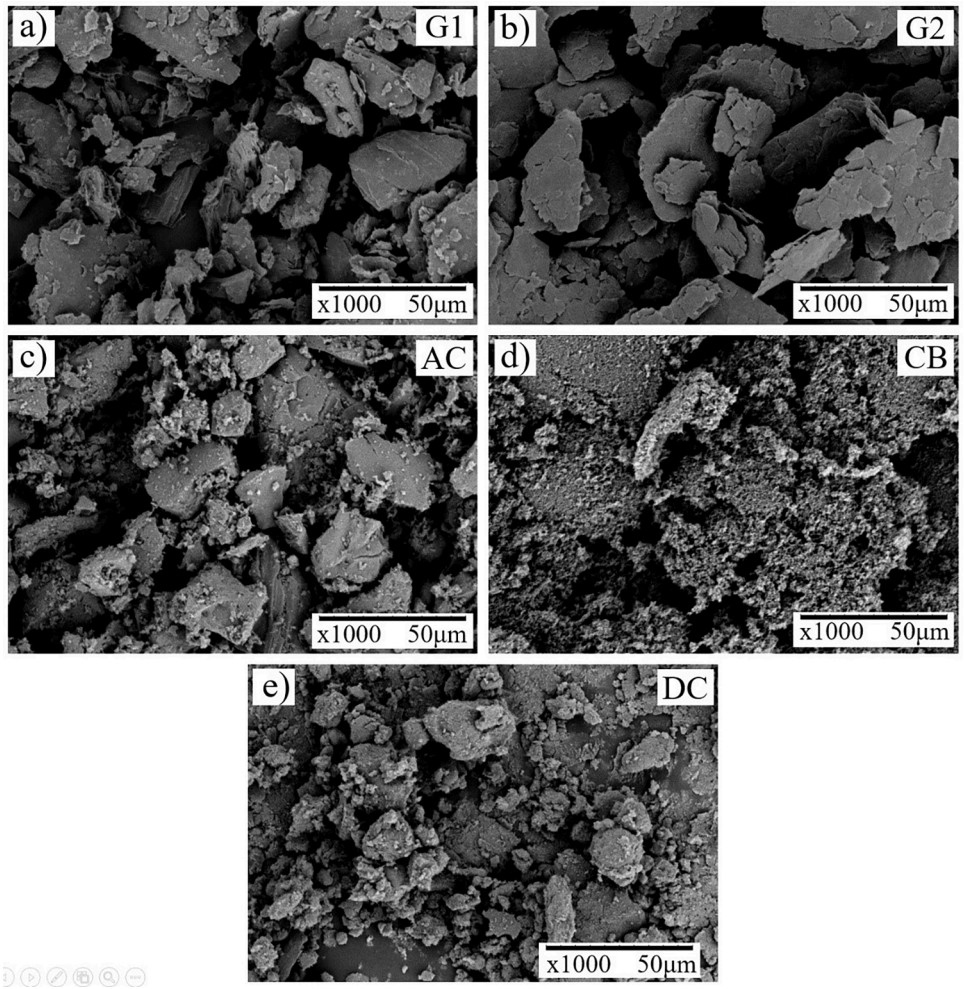

Fig. A2. Secondary electron images of carbonaceous materials grains: a) industrial graphite G1, b) natural graphite G2, c) commercial activated charcoal, d) carbon black, and e) decolorized charcoal.

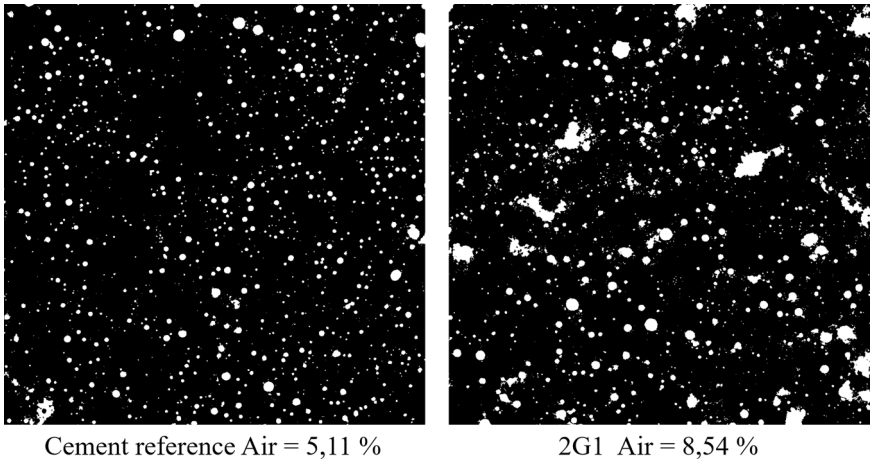

Fig. A3. Binary image of cement mortar (left) and cement with 2 % graphite G1 addition (right).

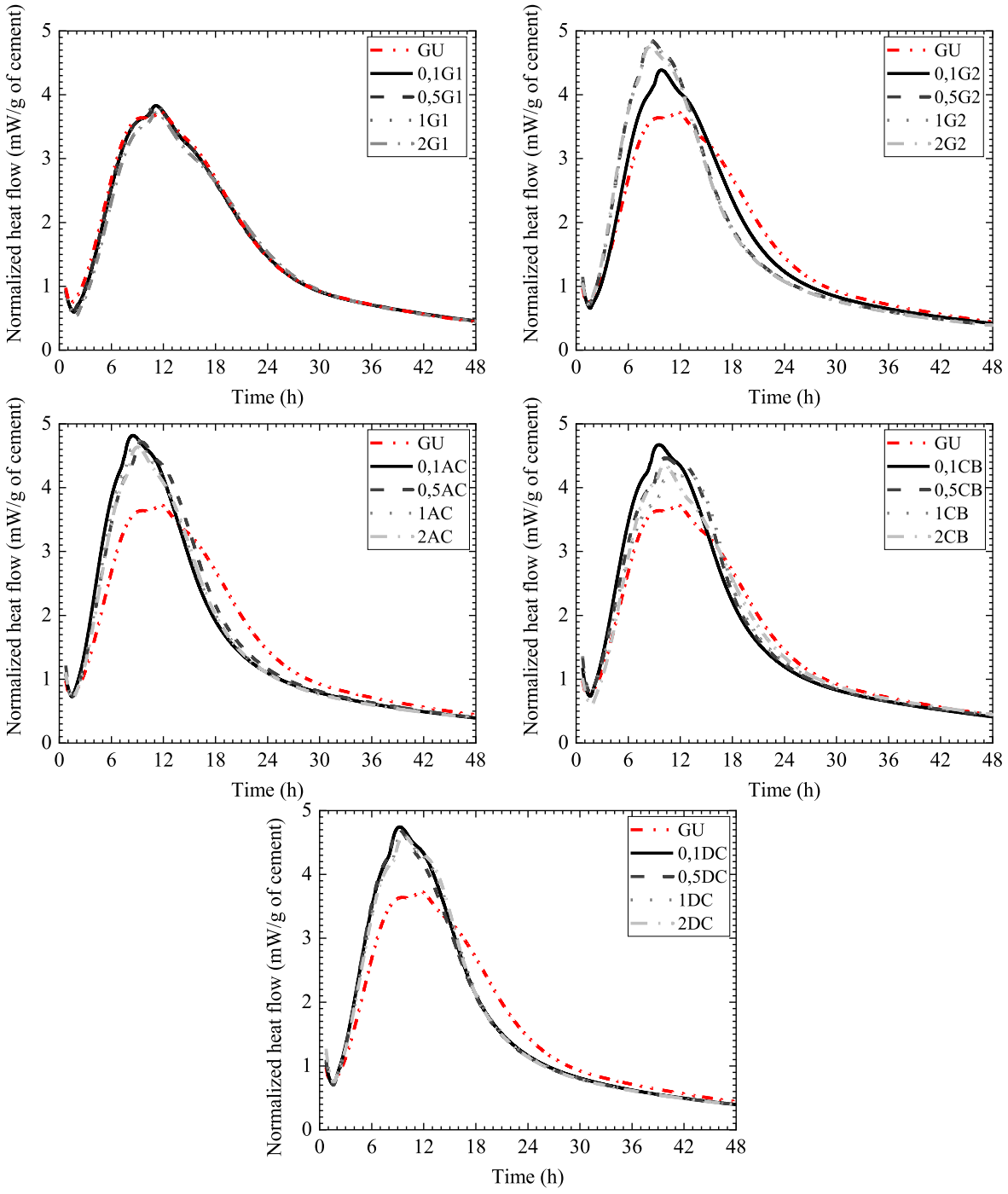

Fig. A4. Isothermal calorimetry curves of cement and cement/carbon pastes.

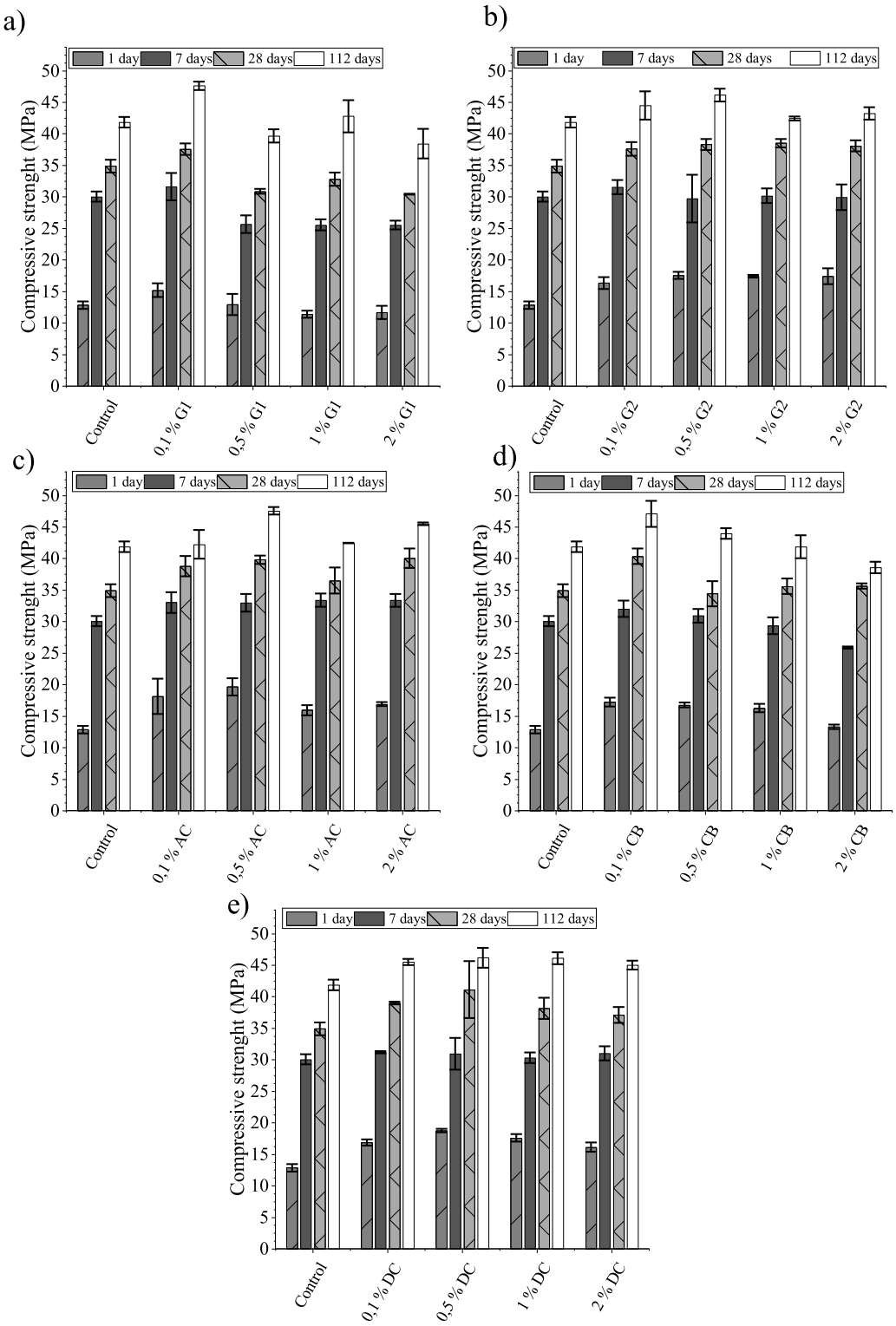

Fig. A5. Compressive strength of mortar samples a) graphite G1, b) graphite G2, c) Activated charcoal AC, d) carbon black CB, e) decolorized charcoal DC at 1, 7, 28 and 112 days.

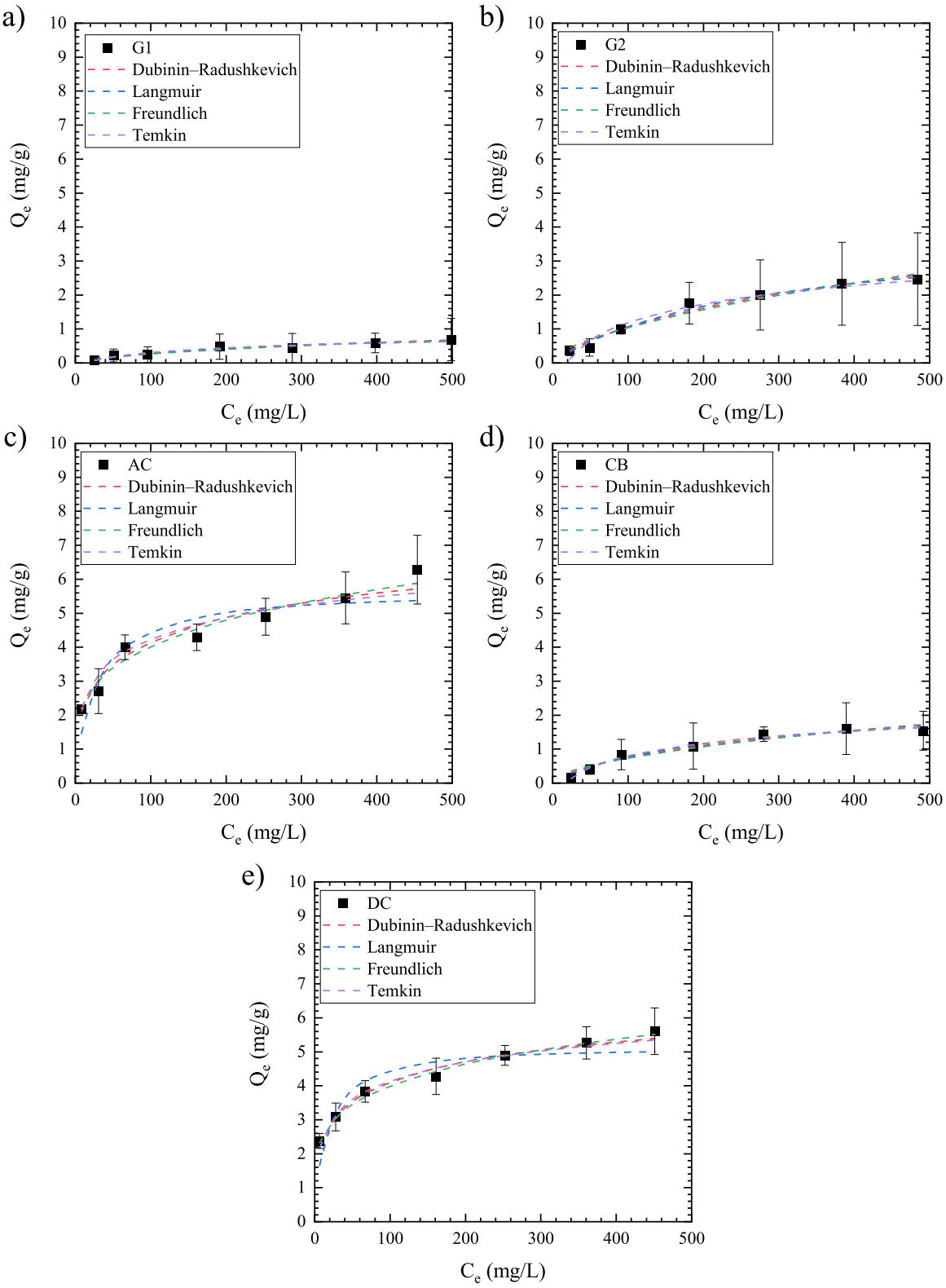

Fig. A6. Isotherm adsorption results for a) graphite G1, b) graphite G2, c) Activated charcoal AC, d) carbon black CB, e) decolorized charcoal DC.

References

[1] Supriya, R. Chaudhury, U. Sharma, P.C. Thapliyal, L.P. Singh, Low-CO2 emission strategies to achieve net zero target in cement sector, J. Clean. Prod. 417 (2023) 137466, https://doi.org/10.1016/j.jclepro.2023.137466.

[2] P.C. Hewlett, M. Liska, Lea's Chemistry of Cement and Concrete, Elsevier, 2019, https://doi.org/10.1016/C2013-0-19325-7.

[3] U.N. Environment, K.L. Scrivener, V.M. John, E.M. Gartner, Eco-efficient cements: potential economically viable solutions for a low-CO2 cement-based materials

industry, Cem. Concr. Res. 114 (2018) 2–26, https://doi.org/10.1016/j.cemconres.2018.03.015.
[4] J. Lehne, F. Preston, Making Concrete Change- Innovation in Low-carbon Cement and Concrete, Chatham House Report, 2018.
[5] V. Brial, H. Tran, L. Sorelli, D. Conciatori, C.M. Ouellet-Plamondon, Evaluation of the reactivity of treated spent pot lining from primary aluminum production as cementitious materials, Resour. Conserv. Recycl. 170 (2021) 105584, https://doi.org/10.1016/j.resconrec.2021.105584.
[6] V. Brial, H. Tran, L. Sorelli, D. Conciatori, C.M. Ouellet-Plamondon, Effect of fluorite addition on the reactivity of a calcined treated spent pot lining in cementitious materials, CEMENT 12 (2023) 100070.
[7] V. Brial, H. Tran, L. Sorelli, D. Conciatori, C.M. Ouellet-Plamondon, Improvement of treated spent pot lining reactivity in cementitious material by calcination, Developments in the Built Environment 12 (2022) 100098.
[8] M. Tokyay, Cement and Concrete Mineral Admixtures, CRC Press, 2016, https://doi.org/10.1201/b20093.
[9] I. Papanikolaou, C. Litina, A. Zomorodian, A. Al-Tabbaa, Effect of natural graphite fineness on the performance and electrical conductivity of cement paste mixes for self-sensing structures, Materials (Basel) 13 (2020) 5833, https://doi.org/10.3390/ma13245833.
[10] S. Wu, P. Wang, B. Li, L. Pang, F. Guo, Study on mechanical and thermal properties of graphite modified cement concrete, Key Eng. Mater. 599 (2014) 84–88, https://doi.org/10.4028/www.scientific.net/KEM.599.84.
[11] Y. Lin, H. Du, Graphene reinforced cement composites: a review, Constr. Build. Mater. 265 (2020) 120312, https://doi.org/10.1016/j.conbuildmat.2020.120312.
[12] C. Liu, X. Huang, Y.Y. Wu, X. Deng, Z. Zheng, Z. Xu, D. Hui, Advance on the dispersion treatment of graphene oxide and the graphene oxide modified cement-based materials, Nanotechnol. Rev. 10 (2021) 34–49, https://doi.org/10.1515/ntrev-2021-0003.
[13] H. Qu, S. Qian, X. Liu, R. Gao, Z. Wang, C. Zheng, Z. Zhang, Carbon dots as a superior building nanomaterial for enhancing the mechanical properties of cement-based composites, J. Build. Eng. 52 (2022) 104523, https://doi.org/10.1016/j.jobe.2022.104523.
[14] C. Bhojaraju, S.S. Mousavi, V. Brial, M. DiMare, C.M. Ouellet-Plamondon, Fresh and hardened properties of GGBS-contained cementitious composites using graphene and graphene oxide, Constr. Build. Mater. 300 (2021) 123902, https://doi.org/10.1016/j.conbuildmat.2021.123902.
[15] X. Tian, H. Hu, Test and study on electrical property of conductive concrete, Procedia Earth and Planetary Sci. 5 (2012) 83–87, https://doi.org/10.1016/j.proeps.2012.01.014.
[16] D.K. Dutta, D. Bordoloi, P.C. Borthakur, Hydration of portland cement clinker in the presence of carbonaceous materials, Cem. Concr. Res. 25 (1995) 1095–1102, https://doi.org/10.1016/0008-8846(95)00104-K.
[17] I. Justo-Reinoso, W.V. Srubar, A. Caicedo-Ramirez, M.T. Hernandez, Fine aggregate substitution by granular activated carbon can improve physical and mechanical properties of cement mortars, Constr. Build. Mater. 164 (2018) 750–759, https://doi.org/10.1016/j.conbuildmat.2017.12.181.
[18] C.F. Ramirez-Gutierrez, R. Arias-Niquepa, J.J. Prías-Barragán, M.E. Rodriguez-Garcia, Study and identification of contaminant phases in commercial activated carbons, J. Environ. Chem. Eng. 8 (2020) 103636, https://doi.org/10.1016/j.jece.2019.103636.
[19] ASTM International, C1738/C1738M-18 Standard Practice For High-Shear Mixing of Hydraulic Cement Pastes, ASTM Standard Book, 2014, pp. 11–13, https://doi.org/10.1520/C1738-11A.2.
[20] C.F. Ferraris, P.E. Stutzman, W.F. Guthrie, J. Winpigler, Certification of SRM 2492: Bingham Paste Mixture for Rheological Measurements, National Institute of Standards and Technology, 2015.
[21] A. Olivas, C.F. Ferraris, W.L. George, E.J. Garboczi, B. Toman, Certification of SRM 2493: Standard Reference Mortar for Rheological Measurements, National Institute of Standards and Technology, 2017, https://doi.org/10.6028/NIST.SP.260-187.
[22] P.-C. Aïtcin, R.J. Flatt, Science and Technology of Concrete Admixtures, Woodhead Publishing, an imprint of Elsevier, Amsterdam, 2016.
[23] ASTM International, C109/C109M − 16a Standard Test Method for Compressive Strength of Hydraulic Cement Mortars Using 2-in . Or [50-mm] Cube Specimens), ASTM Standard Book, 2016, pp. 1–9, https://doi.org/10.1520/C0109.
[24] ASTM International, C305 − 14 Standard Practice For Mechanical Mixing of Hydraulic Cement Pastes and Mortars, ASTM Standard Book, 2015, pp. 14–16, https://doi.org/10.1520/C0305-14.2.
[25] P.C. Fonseca, G.W. Scherer, An image analysis procedure to quantify the air void system of mortar and concrete, Mater. Struct. 48 (2015) 3087–3098, https://doi.org/10.1617/s11527-014-0381-9.
[26] ASTM International, C457/C457M-16 - Standard Test Method for Microscopical Determination of Parameters of the Air-Void System in Hardened Concrete 1, ASTM Standard Book 05, 2016, pp. 1–15, https://doi.org/10.1520/C0457.
[27] ASTM International, C1679-17 - Standard Practice For Measuring Hydration Kinetics of Hydraulic Cementitious Mixtures Using Isothermal Calorimetry, ASTM Standard Book, 2017, p. 16, https://doi.org/10.1520/C1679-17.2.
[28] R. Snellings, J. Chwast, Ö. Cizer, N. De Belie, Y. Dhandapani, P. Durdzinski, J. Elsen, J. Haufe, D. Hooton, C. Patapy, M. Santhanam, K. Scrivener, D. Snoeck, L. Steger, S. Tongbo, A. Vollpracht, F. Winnefeld, B. Lothenbach, Report of TC 238-SCM: hydration stoppage methods for phase assemblage studies of blended cements—Results of a round robin test, Mater. Struct./Materiaux et Construct. 51 (2018), https://doi.org/10.1617/s11527-018-1237-5.
[29] K. Scrivener, R. Snellings, B. Lothenbach, A Practical Guide to Microstructural Analysis of Cementitious Materials, 2016.
[30] K.L. Scrivener, The use of backscattered electron microscopy and image analysis to study the porosity of cement paste, MRS Proceedings 137 (1988) 129–140, https://doi.org/10.1557/proc-137-129.
[31] H.S. Wong, N.R. Buenfeld, Determining the water-cement ratio, cement content, water content and degree of hydration of hardened cement paste: method development and validation on paste samples, Cem. Concr. Res. 39 (2009) 957–965, https://doi.org/10.1016/j.cemconres.2009.06.013.
[32] C.F. Ferraris, K.H. Obla, R. Hill, The influence of mineral admixtures on the rheology of cement paste and concrete, Cem. Concr. Res. 31 (2001) 245–255, https://doi.org/10.1016/S0008-8846(00)00454-3.
[33] H. Vikan, H. Justnes, Rheology of cementitious paste with silica fume or limestone, Cem. Concr. Res. 37 (2007) 1512–1517, https://doi.org/10.1016/j.cemconres.2007.08.012.
[34] O. Abdulfattah, I.H. Alsurakji, A. El-Qanni, M. Samaneh, M. Najjar, R. Abdallah, I. Assaf, Experimental evaluation of using pyrolyzed carbon black derived from waste tires as additive towards sustainable concrete, Case Studies in Construct. Mater. 16 (2022) e00938, https://doi.org/10.1016/j.cscm.2022.e00938.
[35] D. Wang, Q. Wang, Z. Huang, Investigation on the poor fluidity of electrically conductive cement-graphite paste: experiment and simulation, Mater. Des. 169 (2019) 107679, https://doi.org/10.1016/j.matdes.2019.107679.
[36] A.B. Poole, I. Sims, Concrete Petrography, CRC Press, Boca Raton, 2016, https://doi.org/10.1201/b18688.
[37] T. Luo, Q. Wang, Effects of graphite on electrically conductive cementitious composite properties: a review, Materials (Basel) 14 (2021) 4798, https://doi.org/10.3390/ma14174798.
[38] N. Flores Medina, M. del Mar Barbero-Barrera, F. Jové-Sandoval, Improvement of the mechanical and physical properties of cement pastes and mortars through the addition isostatic graphite, Constr. Build. Mater. 189 (2018) 898–905, https://doi.org/10.1016/j.conbuildmat.2018.09.055.
[39] R.C.A. Pinto, K.C. Hover, Frost and Scaling Resistance of High-Strength Concrete, Skokie, Illinois, 2001.
[40] S.M. Monteagudo, A. Moragues, J.C. Gálvez, M.J. Casati, E. Reyes, The degree of hydration assessment of blended cement pastes by differential thermal and thermogravimetric analysis. Morphological evolution of the solid phases, Thermochim. Acta 592 (2014) 37–51, https://doi.org/10.1016/j.tca.2014.08.008.
[41] S. Adu-Amankwah, L. Black, J. Skocek, M. Ben Haha, M. Zajac, Effect of sulfate additions on hydration and performance of ternary slag-limestone composite cements, Constr. Build. Mater. 164 (2018) 451–462, https://doi.org/10.1016/j.conbuildmat.2017.12.165.
[42] T.C. Powers, Structure and physical properties of hardened portland cement paste authorized reprint from american ceramic society, J. Am. Ceram. Soc. 41 (1958) 7.
[43] J. Hu, Z. Ge, K. Wang, Influence of cement fineness and water-to-cement ratio on mortar early-age heat of hydration and set times, Constr. Build. Mater. 50 (2014) 657–663, https://doi.org/10.1016/j.conbuildmat.2013.10.011.
[44] E. Berodier, K. Scrivener, Understanding the filler effect on the nucleation and growth of C-S-H, J. Am. Ceram. Soc. 97 (2014) 3764–3773.
[45] J. Wang, X. Guo, Adsorption isotherm models: classification, physical meaning, application and solving method, Chemosphere 258 (2020) 127279, https://doi.org/10.1016/j.chemosphere.2020.127279.
[46] M.A. Al-Ghouti, D.A. Da'ana, Guidelines for the use and interpretation of adsorption isotherm models: a review, J. Hazard. Mater. 393 (2020) 122383, https://doi.org/10.1016/j.jhazmat.2020.122383.
[47] S. Kalam, S.A. Abu-Khamsin, M.S. Kamal, S. Patil, Surfactant adsorption isotherms: a review, ACS Omega 6 (2021) 32342–32348, https://doi.org/10.1021/acsomega.1c04661.
[48] M. Chabani, A. Amrane, A. Bensmaili, Kinetic modelling of the adsorption of nitrates by ion exchange resin, Chem. Eng. J. 125 (2006) 111–117, https://doi.org/10.1016/j.cej.2006.08.014.